INTRODUCTION

Ulcerative colitis (UC) is a chronic inflammatory bowel disease characterized by periods of remission interrupted by episodes of clinical relapse due to recurrent intestinal inflammation (1). The immunopathogenesis of UC reflects a dysregulated interaction among environmental factors, intestinal flora, and genetic susceptibility factors within the immune system, which triggers inflammatory activities in colonic mucosa (2). Increased mucosal vascular permeability is followed by an influx of vast numbers of granulocytes, monocytes/macrophages into the colonic mucosa in active UC (3). The local and infiltrated leukocytes in colonic mucosa produce and release soluble mediators, including proinflammatory cytokines, chemokines, and proteases, which can exacerbate inflammation and tissue injury (2,4,5). Furthermore, there is evolving evidence for peripheral blood granulocytes and monocytes as being major factors in the immunopathogenesis of UC (2,6). Accordingly, patients with active UC may harbor an elevated peripheral granulocyte (7,8) with activation behavior (6) and prolonged survival time (9). Furthermore, UC is exacerbated and perpetuated by cytokines such as tumor necrosis factor-α, IL (interleukin)-1β, IL-6, and IL-12, which are strongly proinflammatory (10,11) and are released by granulocytes and monocytes as well (5,12). These cytokines have given rise to the inference that elevated and activated granulocytes and monocytes should be targets of therapy in UC.

Conventional medications including 5-aminosalicylic acid, prednisolone, and immunomodulators such as azathioprine and 6-mercaptopurine have been used for many years in the treatment of UC (13–18). However, the use of these drugs has often been associated with adverse side effects that add to disease complexity (15,17–19). Therefore, there is a need for effective and well-tolerated therapies for UC.

Granulocyte and monocyte adsorptive apheresis (GMA) is an extracorporeal therapy that is performed with the Adacolumn (JIMRO, Takasaki, Japan), which selectively depletes granulocytes and monocytes from peripheral blood (8). A number of studies have reported the therapeutic efficacy of GMA in patients with UC, Crohn's disease, and rheumatoid arthritis (20–22). In patients with UC, up to now, most physicians have relied on weekly, one GMA session per week, and in spite of reporting 60–80% efficacy outcomes, the effects take several weeks to be observed (23). With this in mind, we had the impression that an intensive course of GMA should produce a more rapid efficacy compared with weekly GMA. Initially, we undertook a pilot study that showed that rapid remission could be achieved by intensive GMA (24). We have now expanded this idea to the present large, prospective, randomized, multicenter study to evaluate the safety, efficacy, and time to remission of intensive GMA, alongside the routine weekly GMA treatment in patients with active, mild-to-moderate UC.

METHODS

This was an open-label, prospective, randomized, multicenter study aimed at evaluating the clinical efficacy, safety, and the appropriate treatment schedule for GMA in patients with mild-to-moderately active UC. The study was conducted at 24 medical institutions from January 2004 to November 2005; 15 were academic, university institutes, 4 were municipal hospital centers, and 5 were private community clinics. All centers had adequate experience to perform GMA for the treatment of UC. The protocol and patients' informed consent forms were reviewed and approved by an Institutional Review Board at each study center before the study. The study was conducted in accordance with the Declaration of Helsinki, in compliance with the consolidated Good Clinical Practice guidelines and the applicable regulatory requirements.

Patient population

Male or nonpregnant female UC patients older than 12 years were eligible if they had newly diagnosed or relapsing mild-to-moderately active disease. The severity of UC was assessed by the clinical activity index (CAI) according to Lichtiger *et al.* (25). Patients who had a CAI score from 5 to 12 were classified as having mild-to-moderately active UC (25) and were enrolled. An endoscopy that visualized the extent of disease within the previous 6 months was necessary.

Patients with granulocytopenia (neutrophil count $<2{,}000$ per μl), serious heart or kidney disease, coagulation disorder, and infection were excluded. Oral maintenance treatment was permitted if given at a stable dose for at least 2 weeks before inclusion for 5-aminosalicylic acid and for at least 8 weeks for azathioprine/6-mercaptopurine. Concomitant medications used for diseases other than UC, which did not violate the protocol inclusion, were allowed.

Assignment

After screening and enrollment for this study, patients were randomly assigned to weekly GMA or intensive GMA, two sessions per week, in a 1:1 ratio. Randomization was based on a central computer-generated scheme that assigned the eligible patient to the next randomization for the concerned center.

Treatment

GMA treatment was performed as previously described (20,21,26). Briefly, Adacolumns and blood circuit lines were primed with sterile saline to remove air bubbles from the column and flow lines, and a second priming of the system was carried out with heparinized saline. Blood access was through the antecubital vein in one arm and from the outflow, blood returned to the patient through the antecubital vein in the contralateral arm. The duration of one GMA session was 60 min at a flow rate of 30 ml/min as per protocol. Treatment was carried out partly in outpatient facilities and partly in hospital facilities.

Patients in weekly GMA received one treatment per week and those in intensive GMA received two treatments per week. The maximum number of treatments that was allowed was 10. However, when patients achieved remission, GMA was discontinued. The treatment/observation period was 70 days in weekly GMA and 35 days in intensive GMA.

With respect to the UC disease status, each patient was evaluated by Lichtiger's CAI at screening, baseline, and then before each GMA session. Similarly, the GMA performance condition was recorded at each study visit.

Outcomes

Primary end point: The primary measure of response was clinical remission at the end of the study. Clinical remission was defined as Lichtiger's CAI ≤4. Clinical response was defined as a decrease in CAI by ≥3 points, but that did not reach ≤4. Remission rate was assessed by a per-protocol population analysis.

Secondary end points: The time to remission when a patient achieved remission was compared between the two groups. Analysis of time to remission was carried out by a life-table analysis using the method of Kaplan and Meier. Statistical comparison was carried out by the log-rank test. The incidence and severity of adverse side effects were also analyzed.

Statistical analysis

When appropriate, data are presented as mean±s.e. values. For statistical analysis, data were processed using SAS software (SAS Institute, Cary, NC). Data analysis was carried out with the Wilcoxon signed rank test or as otherwise indicated in figure or table legends. $P<0.05$ was considered statistically significant.

Determination of sample size. This trial was designed as a superiority study. To show a statistical difference in the remission rate between an assumption of 60% in weekly GMA and 80% in intensive GMA, with a first-kind error of 5% and a power of 80%, a sample size of 81 patients per each group in the per-protocol population was estimated. With a 15% withdrawal, a total of 100 patients had to be included in each group.

RESULTS

Participant flow and follow-up

A total of 163 patients met the study inclusion criteria and were randomized to weekly GMA ($n=79$) and intensive GMA ($n=84$). As outlined in **Figure 1**, 3 patients in weekly GMA and 11 patients in intensive GMA could not be included in the efficacy analysis. Of the three cases that were excluded in weekly GMA, two had reached CAI values >12 at baseline (an exclusion item), and one had CAI <4 at baseline. Similarly, the 11 excluded cases in intensive GMA had baseline CAI values >12, had newly added concomitant medication (an exclusion item), were younger than 12 years of age, or their interim follow-up was not sufficient. Therefore, a total of 149 cases (76 cases in weekly GMA and 73 cases in intensive GMA) were available for efficacy evaluations. There was no significant difference between the two groups with respect to patients' gender, age, inpatients/outpatients, duration of UC, and CAI. Past or concomitant conventional pharmacological agents used by these patients were salazosulfapyridine, 5-aminosalicylic acid, prednisolone, azathioprine, or 6-mercaptopurine. All patients who were on one or more of these medications had shown inadequate response and there was no significant difference between the two groups with respect to past or concomitant use of these medications. Full patients' demography is presented in **Table 1**.

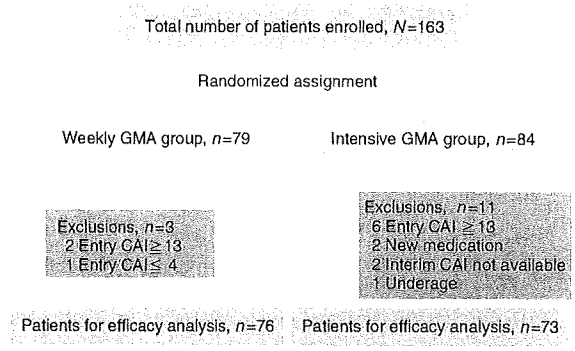

Figure 1. Flowchart of patients enrolled in the study. CAI, clinical activity index; GMA, granulocyte and monocyte adsorptive apheresis.

Table 1. Baseline demographics of patients in weekly or intensive GMA

Characteristic	Weekly GMA ($n=76$)	Intensive GMA ($n=73$)	*P* value
Sex (male: female)	47:29	42:31	0.59
Age (years; range)	37.8 (15–75)	41.6 (17–78)	0.13
Body weight (kg; mean±s.e.)	55.7±9.3	56.6±11.2	0.62
Duration of UC (months; range)	90.6 (1–444)	86.5 (1–312)	0.65
UC extension (total colitis: left-sided colitis: proctitis)	37:39:0	36:36:1	0.57
Inpatient: outpatient	31:45	39:33	0.10
Average CAI (mean±s.e.)	9.8±1.7	9.3±1.9	0.08
Use of salfasalazopyrine/5-ASA	74	67	0.41
Use of steroids	74	72	0.96
Average steroid dose (PSL; mg/day mean±s.e.)	12.5±3.2	13.8±4.0	0.49
Use of AZA/6-MP	17	16	0.98

5-ASA, 5-aminosalicylic acid; CAI, clinical activity index; GMA, granulocyte and monocyte adsorptive apheresis; 6-MP, 6-mercaptopurine; PSL, prednisolone; UC, ulcerative colitis.
By χ^2 test or Fisher's exact test.

Primary efficacy evaluation

As stated above, 76 of 79 patients randomized to weekly GMA and 73 of 84 patients randomized to intensive GMA were available for efficacy assessment as per protocol. During the 70 days of study period in weekly GMA, 41 of 76 patients (54.0%) achieved clinical remission, whereas during the 35 days of the study period in intensive GMA, 52 of 73 patients (71.2%) achieved clinical remission ($P=0.029$). Therefore, intensive GMA was associated with a significantly higher remission rate compared with routine weekly GMA.

All of the 79 patients randomized to weekly GMA and 82 of the 84 patients randomized to intensive GMA were available for intention-to-treat analysis. The two patients who were excluded had not been treated with GMA and were not included in the intention-to-treat analysis. The intention-to-treat analysis showed that 43 of 79 patients (54.4%) achieved clinical remission in weekly GMA, and 57 of 82 patients (69.5%) achieved clinical remission in intensive GMA ($P=0.047$).

Secondary efficacy evaluation

The changes in the cumulative remission rate among patients in weekly and intensive GMA are shown in **Figure 2**. The mean time to remission among 41 patients in weekly GMA who achieved clinical remission was 28.1±16.9 days, whereas the mean time to remission in 52 patients of intensive GMA who achieved clinical remission was 14.9±9.5 days ($P<0.0001$). Therefore, intensive GMA was associated with rapid remission as compared with routinely applied weekly GMA.

Safety and tolerability

No device-related serious adverse event or unexpected adverse event was observed in either group. Similar to previous studies (27), adverse events were consistent with those generally acknowledged to accompany extracorporeal procedures (such as nausea, flushing, lightheadedness, and dizziness). A total of 31 adverse events in weekly GMA ($n=14$) and intensive GMA ($n=17$) were observed ($P=0.88$). Adverse incidents in 11 of 14 cases in weekly GMA and 13 of 17 cases in intensive GMA were considered to be likely treatment related. None of these adverse events was serious and did not require medication or a discontinuation of GMA treatment. No episode of opportunistic infection was observed in either group, suggesting that depletion of large quantities of leukocytes by GMA would not lead to immunodeficiency. Furthermore, both intensive and weekly GMA treatments were well tolerated by patients and there were no technical problems.

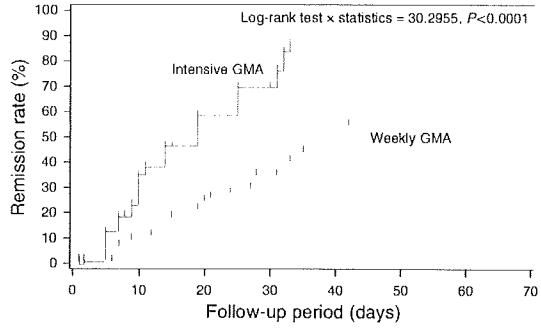

Figure 2. Cumulative remission rates of routine granulocyte and monocyte adsorptive apheresis (GMA) therapy (one GMA session weekly) and intensive GMA (two GMA sessions per week) shown using the Kaplan–Meier method. Intensive GMA, bold lines; weekly GMA, dotted lines. During the 70 days of the study period in weekly GMA, 41 of 76 patients (54.0%) achieved clinical remission (clinical activity index ≤4), whereas during the 35 days of the study period in intensive GMA, 52 of 73 patients (71.2%) achieved clinical remission ($P=0.029$). Furthermore, the mean time to remission for 41 patients in weekly GMA who achieved clinical remission was 28.1±16.9 days vs. 14.9±9.5 days in 52 patients of group B ($P<0.001$). Patients who dropped out during the study because of exacerbating disease are regarded as censored, as shown by the tick on the line.

DISCUSSION

In this study, we have shown that intensive treatment with GMA was more effective in mild-to-moderately active UC compared with conventional weekly GMA. Furthermore, induction of remission was rapidly achieved with intensive GMA without increasing the incidence of side effects.

Activated granulocytes and monocytes/macrophages are known to produce an array of pleiotropic cytokines that can exacerbate and perpetuate mucosal inflammation (5,7,12). Hence, depleting excess and activated granulocytes and monocytes by GMA should alleviate inflammation and promote remission of active UC. On the basis of this idea, this multicenter study was undertaken to better understand the therapeutic potential of GMA. The study was designed to have the routinely used weekly one GMA session as a standard treatment with known clinical efficacy (20,28). Efficacy assessment as per protocol showed a remission rate of 54.0% for weekly (one GMA session per week) and 71.2% for intensive GMA (two sessions per week). The mean time to remission in the intensive GMA group was shortened to approximately half of that in the weekly GMA group. This was consistent with our preliminary pilot study (24). Hence, intensive GMA was associated with both a shortening of morbidity time and a higher rate of efficacy. Intensive GMA seemed to be safe, no serious adverse event was observed in either group, and patients' compliance was excellent. Similarly, no increase in complications related to GMA was observed.

Since its clinical application, GMA has been routinely used once a week for a duration of 5–10 weeks. This treatment schedule has achieved a clinical response rate of 50–80% by a number of researchers, and has been assigned as the standard regimen of GMA by the Japanese Ministry of Labor and Welfare. However, the duration to achieve remission was 3–5 weeks in the majority of patients, which was relatively long compared with corticosteroids and other medications. The results of our pilot trial suggested that there might be a frequency-dependent or dose-dependent response in GMA. This study was designed to seek the optimal treatment schedule of GMA in a more powerful, multicenter, randomized, control trial. The results of our

study further strengthen the notion that the efficacy of GMA is frequency dependent. On the basis of the idea of dose dependency, we are conducting a trial in which GMA is performed for 120 min instead of the routine 60 min. Preliminary results indicate that when GMA processes a larger volume of blood, it may show more efficacy. Furthermore, by decreasing the duration to achieve remission, intensive GMA may be an alternative for the treatment of severe active UC, wherein prolonged morbidity is not desirable. However, as this study was an open-label study, we need to confirm these results in a double-blinded placebo-controlled study.

Recently, Sands *et al.* (27) conducted a large, randomized, sham-controlled study of GMA for active UC. The results of their study failed to show the efficacy of GMA. The rate of remission, defined by a Mayo score of 0–2, was 17% for GMA and 11% for sham-apheresis. The overall low rate of remission in their study is because of the different criteria of remission that were applied. Their protocol was more similar to the standard weekly schedule, which may have limited the efficacy of GMA. There was even a week in which no treatment was performed in the middle of the schedule, which could have affected the results. Taking into account that there may be a frequency-dependent and dose-dependent effect in GMA, we suggest that a more intensive treatment schedule, in which the processed volume of blood is adjusted on the basis of the weight of the patient, be applied to seek the efficacy of GMA in a double-blinded placebo-controlled study.

Basic research studies have shown that GMA not only quantitatively depletes granulocytes/monocytes from peripheral blood but also induces qualitative changes in leukocytes. We have recently shown that GMA modulates the function of monocyte-derived dendritic cells (29). Monocyte/dendritic cells are potent antigen-presenting cells that continuously migrate to the inflamed intestine. Repetitive depletion of inflammatory monocytes/dendritic cells by intensive GMA may account for the high efficacy of intensive GMA.

In conclusion, an intensive GMA treatment of patients with active UC was more efficacious than was the routine weekly GMA, and induced rapid remission in the majority of patients with mild-to-moderately active UC. Placebo/sham-controlled trials are required to confirm the results of our study.

ACKNOWLEDGMENTS

The authors thank Toru Takebayashi for essential advice in study design.

CONFLICT OF INTEREST

Guarantor of the article: Toshifumi Hibi, MD, PhD.

Specific author contributions: Conception and design, patient recruitment, acquisition, analysis, and data interpretation, and writing of the paper: Atsushi Sakuraba; conception and design and patient recruit: Toshiyuki Matsui, Yasuo Suzuki, and Akira Andoh; patient recruitment: Satoshi Motoya, Kenji Watanabe, Masakazu Nishishita, Kazunari Kanke, Tadayuki Oshima, Reiko Kunisaki, Takayuki Matsumoto, Hiroyuki Hanai, Ken Fukunaga, Naoki Yoshimura, Toshimi Chiba, Shinsuke Funakoshi, Nobuo Aoyama, Hiroshi Nakase, Yohei Mizuta, Ryoichi Suzuki, Taiji Akamatsu, Masahiro Iizuka, and Toshifumi Ashida; conception and design, patient recruitment, acquisition, analysis, and data interpretation: Toshifumi Hibi.

Financial support: One Adacolumn per week in the intensive GMA group was provided by JIMRO to Keio University School of Medicine, Hyogo College of Medicine, and Kobe University School of Medicine.

Potential competing interests: None.

Study Highlights

WHAT IS CURRENT KNOWLEDGE

- ✓ Granulocyte and monocyte adsorptive apheresis (GMA), applied weekly for 10 weeks, induces remission in approximately 60–80% of active ulcerative colitis.
- ✓ The optimal treatment schedule of GMA remains unclear.

WHAT IS NEW HERE

- ✓ Intensive GMA, with 2 sessions per week, was more efficacious than weekly GMA.
- ✓ Intensive GMA shortened the time to remission compared with weekly GMA.
- ✓ The efficacy of GMA may be frequency dependent.

REFERENCES

1. Hendrickson BA, Gokhale R, Cho JH. Clinical aspects and pathophysiology of inflammatory bowel disease. Clin Microbiol Rev 2002;15:79–94.
2. Xavier RJ, Podolsky DK. Unravelling the pathogenesis of inflammatory bowel disease. Nature 2007;448:427–34.
3. Bjarnason I, MacPherson A, Hollander D. Intestinal permeability: an overview. Gastroenterology 1995;108:1566–81.
4. Lloyd AR, Oppenheim JJ. Poly's lament: the neglected role of the polymorphonuclear neutrophil in the afferent limb of the immune response. Immunol Today 1992;13:169–72.
5. Cassatella MA, Meda L, Gasperini S *et al.* Interleukin-12 production by human polymorphonuclear leukocytes. Eur J Immunol 1995;25:1–5.
6. McCarthy DA, Rampton DS, Liu YC. Peripheral blood neutrophils in inflammatory bowel disease: morphological evidence of in vivo activation in active disease. Clin Exp Immunol 1991;86:489–93.
7. Meuret G, Bitzi A, Hammer B. Macrophage turnover in Crohn's disease and ulcerative colitis. Gastroenterology 1978;74:501–3.
8. Saniabadi AR, Hanai H, Takeuchi K *et al.* Adacolumn, an adsorptive carrier based granulocyte and monocyte apheresis device for the treatment of inflammatory and refractory diseases associated with leukocytes. Ther Apher Dial 2003;7:48–59.
9. Brannigan AE, O'Connell PR, Hurley H *et al.* Neutrophil apoptosis is delayed in patients with inflammatory bowel disease. Shock 2000;13:361–6.
10. Papadakis KA, Targan SR. Role of cytokines in the pathogenesis of inflammatory bowel disease. Annu Rev Med 2000;51:289–98.
11. Schreiber S, Nikolaus S, Hampe J *et al.* Tumour necrosis factor alpha and interleukin 1beta in relapse of Crohn's disease. Lancet 1999;353:459–61.
12. Nikolaus S, Bauditz J, Gionchetti P *et al.* Increased secretion of pro-inflammatory cytokines by circulating polymorphonuclear neutrophils and regulation by interleukin 10 during intestinal inflammation. Gut 1998;42:470–6.
13. Schroeder KW, Tremaine WJ, Ilstrup DM. Coated oral 5-aminosalicylic acid therapy for mildly to moderately active ulcerative colitis. A randomized study. N Engl J Med 1987;317:1625–9.
14. Rachmilewitz D, Karmeli F, Schwartz LW *et al.* Effect of aminophenols (5-ASA and 4-ASA) on colonic interleukin-1 generation. Gut 1992;33:929–32.

15. Hanauer SB, Stathopoulos G. Risk-benefit assessment of drugs used in the treatment of inflammatory bowel disease. Drug Saf 1991;6:192–219.
16. Gionchetti P, Rizzello F, Habal F *et al.* Standard treatment of ulcerative colitis. Dig Dis 2003;21:157–67.
17. Card T, West J, Hubbard R *et al.* Hip fractures in patients with inflammatory bowel disease and their relationship to corticosteroid use: a population based cohort study. Gut 2004;53:251–5.
18. Kornbluth A, Marion JF, Salomon P *et al.* How effective is current medical therapy for severe ulcerative and Crohn's colitis? An analytic review of selected trials. J Clin Gastroenterol 1995;20:280–4.
19. Taffet SL, Das KM. Sulfasalazine. Adverse effects and desensitization. Dig Dis Sci 1983;28:833–42.
20. Shimoyama T, Sawada K, Hiwatashi N *et al.* Safety and efficacy of granulocyte and monocyte adsorption apheresis in patients with active ulcerative colitis: a multicenter study. J Clin Apher 2001;16:1–9.
21. Fukuda Y, Matsui T, Suzuki Y *et al.* Adsorptive granulocyte and monocyte apheresis for refractory Crohn's disease: an open multicenter prospective study. J Gastroenterol 2004;39:1158–64.
22. Fujimori J, Yoshino S, Koiwa M *et al.* Improvement in rheumatoid arthritis following application of an extracorporeal granulotrap column, G-1. Rheumatol Int 1996;15:175–80.
23. Hibi T, Sakuraba A. Is there a role for apheresis in gastrointestinal disorders? Nat Clin Pract Gastroenterol Hepatol 2005;2:200–1.
24. Sakuraba A, Sato T, Naganuma M *et al.* A pilot open-labeled prospective randomized study between weekly and intensive treatment of granulocyte and monocyte adsorption apheresis for active ulcerative colitis. J Gastroenterol 2008;43:51–6.
25. Lichtiger S, Present DH, Kornbluth A *et al.* Cyclosporine in severe ulcerative colitis refractory to steroid therapy. N Engl J Med 1994;330:1841–5.
26. Naganuma M, Funakoshi S, Sakuraba A *et al.* Granulocytapheresis is useful as an alternative therapy in patients with steroid-refractory or -dependent ulcerative colitis. Inflamm Bowel Dis 2004;10:251–7.
27. Sands BE, Sandborn WJ, Feagan B *et al.* A randomized, double-blind, sham-controlled study of granulocyte/monocyte apheresis for active ulcerative colitis. Gastroenterology 2008;135:400–9.
28. Maiden L, Takeuchi K, Baur R *et al.* Selective white cell apheresis reduces relapse rates in patients with IBD at significant risk of clinical relapse. Inflamm Bowel Dis 2008;14:1413–8.
29. Iwakami Y, Sakuraba A, Takada Y *et al.* Granulocyte and monocyte adsorption apheresis modulates monocyte dereived dendritic cell function in patients with active ulcerative colitis. Ther Apher Dial 2009;13:138–46.

Smad2 and Smad3 Phosphorylated at Both Linker and COOH-Terminal Regions Transmit Malignant TGF-β Signal in Later Stages of Human Colorectal Cancer

Koichi Matsuzaki,[1] Chiaki Kitano,[4] Miki Murata,[1] Go Sekimoto,[1] Katsunori Yoshida,[1] Yoshiko Uemura,[2] Toshihito Seki,[1] Shigeru Taketani,[4] Jun-ichi Fujisawa,[3] and Kazuichi Okazaki[1]

Departments of [1]Gastroenterology and Hepatology, [2]Surgical Pathology, and [3]Microbiology, Kansai Medical University, Osaka, Japan; and [4]Department of Biotechnology, Kyoto Institute of Technology, Kyoto, Japan

Abstract

Transforming growth factor (TGF)-β initially inhibits growth of mature epithelial cells. Later, however, autocrine TGF-β signaling acts in concert with the Ras pathway to induce a proliferative and invasive phenotype. TGF-β activates not only TGF-β type I receptor (TβRI) but also Ras-associated kinases, which differentially phosphorylate the mediators Smad2 and Smad3 to create distinct phosphorylated forms: COOH-terminally phosphorylated Smad2/3 (pSmad2C and pSmad3C) and both linker and COOH-terminally phosphorylated Smad2/3 (pSmad2L/C and pSmad3L/C). In this study, we investigated actions of pSmad2L/C and pSmad3L/C in cancer progression. TGF-β inhibited cell growth by down-regulating c-Myc oncoprotein through the pSmad2C and pSmad3C pathway; TGF-β signaling, in turn, enhanced cell growth by up-regulating c-Myc through the cyclin-dependent kinase (CDK) 4–dependent pSmad2L/C and pSmad3L/C pathways in cell nuclei. Alternatively, TβRI and c-Jun NH_2-terminal kinase (JNK) together created cytoplasmic pSmad2L/C, which entered the nucleus and stimulated cell invasion, partly by up-regulating matrix metalloproteinase-9. In 20 clinical samples, pSmad2L/C and pSmad3L/C showed nuclear localization at invasion fronts of all TGF-β–producing human metastatic colorectal cancers. *In vitro* kinase assay confirmed that nuclear CDK4 and cytoplasmic JNK obtained from the tumor tissue could phosphorylate Smad2 or Smad3 at their linker regions. We suggest that CDK4, together with JNK, alters tumor-suppressive TGF-β signaling to malignant characteristics in later stages of human colorectal cancer. The linker phosphorylation of Smad2 and Smad3 may represent a target for intervention in human metastatic cancer. [Cancer Res 2009;69(13):5321–30]

Introduction

Transforming growth factor (TGF)-β, a potent inhibitor of epithelial cell growth, acts as a tumor suppressor in early cancer. In later stages of cancer, however, TGF-β interacts with the Ras pathway to induce an epithelial-mesenchymal transition toward an invasive and metastatic tumor phenotype (1–3). Tumor-promoting effects of TGF-β have been shown by the ability of agents that block TGF-β signaling to inhibit invasiveness of cancer cell lines *in vitro* and their metastatic potential *in vivo* (4–6) and by data showing that TGF-β can directly stimulate growth and motility of cancer cells (7). Mechanisms by which TGF-β acts both to promote and inhibit tumor progression have been extensively studied but remain unclear.

Smads, central mediators converting signals from receptors for TGF-β superfamily members to the nucleus (8), are modular proteins with conserved Mad homology (MH) 1, intermediate linker, and MH2 domains (9). Catalytically active TGF-β type I receptor (TβRI) phosphorylates the COOH-terminal serine residues of receptor-activated Smads (10), which include Smad2 and the highly similar protein Smad3. The linker domain undergoes regulatory phosphorylation by Ras-associated kinases, including extracellular signal-regulated kinase (ERK), c-Jun NH_2-terminal kinase (JNK), and cyclin-dependent kinase (CDK) 4 (11–13). TβRI and Ras-associated kinases differentially phosphorylate Smad2 and Smad3 to create three phosphorylated forms: COOH-terminally phosphorylated Smad2/3 (pSmad2C and pSmad3C), linker phosphorylated Smad2/3 (pSmad2L and pSmad3L), and both linker and COOH-terminally phosphorylated Smad2/3 (pSmad2L/C and pSmad3L/C; refs. 14, 15). Phosphorylated Smad2 and Smad3 rapidly oligomerize with Smad4 and translocate to the nucleus, where they regulate transcription of target genes (16).

Reversible shifting of Smad3-mediated signaling between tumor suppression and oncogenesis in hyperactive Ras-expressing epithelial cells indicates that TβRI-dependent pSmad3C transmits a tumor-suppressive TGF-β signal, whereas oncogenic features such as cell growth and invasion are promoted through the JNK-dependent pSmad3L pathway (17, 18). Linker phosphorylation of Smad3 indirectly inhibits its COOH-terminal phosphorylation and subsequently suppresses tumor-suppressive pSmad3C signaling (Supplementary Fig. S1). TGF-β signaling confers a selective advantage on tumor cells by shifting from a tumor-suppressive TβRI/pSmad3C pathway to an oncogenic JNK/pSmad3L pathway during sporadic human colorectal carcinogenesis (19), an observation that has been extended to hepatic carcinogenesis (20–22). However, the biological significance of pSmad2L/C and pSmad3L/C remains unknown (15).

In this study, we investigated the role of pSmad2L/C and pSmad3L/C in cancer progression. Based on our findings, we conclude that perturbation of autocrine TGF-β signaling by nuclear CDK4 and cytoplasmic JNK accounts for the critical role of Smad in the malignant cell behavior characterizing advanced stages of human cancer.

Note: Supplementary data for this article are available at Cancer Research Online (http://cancerres.aacrjournals.org/).

Requests for reprints: Koichi Matsuzaki, Department of Gastroenterology and Hepatology, Kansai Medical University, 10-15 Fumizonocho, Moriguchi, Osaka 570-8506, Japan. Phone: 81-6-6992-1000, ext. 41201; Fax: 81-6-6996-4874; E-mail: matsuzak@takii.kmu.ac.jp.

doi:10.1158/0008-5472.CAN-08-4203

Materials and Methods

Generation of mouse embryo-derived fibroblasts. Cells from several Smad3 wild-type (*Smad3*$^{+/+}$) and knockout (*Smad3*$^{\Delta ex8/\Delta ex8}$) littermate embryos (23) were pooled by genotype to generate fibroblasts, which were used for experiments as mouse embryo-derived fibroblasts (MEF) after three passages. Smad2$^{-/-}$ MEFs were provided by Dr. A. Roberts (National Cancer Institute).

Cell culture. ACBRI 519 human intestinal epithelial cells and COLO320 human colon cancer cells were obtained from Applied Cell Biology Research Institute and Health Science Research Resources Bank, respectively. ACBRI 519 cells were sensitive to growth inhibition by TGF-β and COLO320 cells were resistant (24). Smad2$^{-/-}$ and Smad3$^{-/-}$ MEFs were used for infection experiments.

Domain-specific antibodies against phosphorylated Smad2 and Smad3. Nine polyclonal anti-phospho-Smad2 and anti-phospho-Smad3 sera were raised against the phosphorylated linker and COOH-terminal regions of Smad2 and Smad3 by immunization of rabbits with synthetic peptides (Supplementary Fig. S2; ref. 17). Relevant antisera were affinity purified using the phosphorylated peptides as described previously (25).

Constructs. Flag-tagged wild-type or CDK/JNK phosphorylation mutants of Smad2 and Smad3 were inserted into a retroviral vector (pQCXIN; Clontech) containing a puromycin resistance marker as described previously (17).

Retroviral infection and expression of Flag-tagged Smad2 and Smad3 mutants. Smad2$^{-/-}$ or Smad3$^{-/-}$ MEFs were infected with retroviral solutions carrying Flag-tagged Smad2 or Smad3 mutants lacking phosphorylation sites in the linker and/or COOH-terminal regions as described previously (17).

Immunoprecipitation and immunoblotting. Immunoprecipitation and immunoblotting were performed as described previously (12, 17). Where indicated, cells were pretreated with a JNK inhibitor SP600125 (Calbiochem), a TβRI inhibitor SB431542 (Calbiochem), or a CDK4 inhibitor (Calbiochem) for 2 h before adding TGF-β or platelet-derived growth factor (PDGF). To detect pSmad2L/C and pSmad3L/C, nuclear extracts were immunoprecipitated with anti-pSmad2/3C antibody and the immunoprecipitates were immunoblotted using anti-pSmad2/3L antibody. Immunoblots were also analyzed using 1 μg/mL anti-c-Myc antibody (Santa Cruz Biotechnology) and 0.1 μg/mL anti-matrix metalloproteinase-9 (anti-MMP-9) antibody (R&D Systems).

Nuclear/cytosolic extracts and *in vitro* kinase assay. Nuclear and cytosolic extracts were prepared according to the manufacturer's protocol (Qiagen). Activated JNK was immunoprecipitated from cytosolic extract with anti-phospho-JNK antibody (Promega). CDK4 was immunoprecipitated from nuclear extract with anti-CDK4 antibody (Millipore). The immune complexes were collected with protein G-Sepharose (GE Healthcare). Bacterial expression and purification of glutathione *S*-transferase (GST)-Smad2 and GST-Smad3 were carried out, and kinase reaction was performed as described previously (12).

Immunohistochemical studies. Immunohistochemical analyses of human liver specimens were performed as described previously (19).

[^{3}H]thymidine incorporation. DNA synthesis was measured by incorporation of 1 μCi/mL [^{3}H]thymidine (GE Healthcare) into 5% trichloroacetic acid–precipitable material after a 4-h pulse exposure as described previously (12).

Matrigel invasion assay. Membranes with 8-μm pores covered with Matrigel (BD Biosciences) on the upper surface were coated with type I collagen on the lower side. Where indicated, cells were pretreated with a MMP-2/MMP-9 inhibitor II (Calbiochem) for 1 h before adding TGF-β or PDGF. Infiltrating cells were counted in five randomly selected regions as described previously (17).

Tumor specimens. Pathology reports and histologic slides were reviewed independently by two pathologists at Kansai Medical University Hospital. Sites of cancers included transverse colon (n = 1), sigmoid colon (n = 10), and rectum (n = 9). Tumors were staged at the time of surgery by standard criteria using tumor-node-metastasis–based staging according to the unified international colorectal cancer staging classification (26).

We scored pSmad2 and pSmad3 positivity in cell nuclei as follows: 0, no positivity; 1, <25% of nuclei showing positivity; 2, from 25% to 50%; 3, from 50% to 75%; 4, >75% (20, 21). Written informed consent was obtained from each patient according to the Helsinki Declaration. We also obtained approval for this study from our institutional ethics committee.

Reverse transcription-PCR. Isolation of RNA, RT, and PCR of TGF-β type II receptor (27, 28); Smad2 (29); and Smad4 (30) was performed as described previously (19).

Results

TGF-β signaling converts JNK-dependent pSmad2L into pSmad2L/C. To investigate the role of individual phosphorylation domains of Smad2 and Smad3, we generated a total of nine antibodies directed at each phosphorylation site in the linker and COOH-terminal regions (Fig. 1*A*; ref. 17). We initially studied the kinetics of Smad2 and Smad3 phosphorylation in MEFs after stimulation by PDGF. PDGF-dependent phosphorylation occurred on one threonine and three serine residues within the linker regions but was not observed at their COOH-terminal regions (Fig. 1*B*). The linker segments serve as substrates for JNK both *in vivo* and *in vitro* at 15 min after PDGF treatment (Fig. 1*C*). TGF-β signal in the presence of PDGF induced an increase in phosphorylation of Smad2L/C: pSmad2L/C appeared at 15 minutes, reached a maximum at 30 minutes, and returned to the basal level by 2 hours (Fig. 1*D*). TGF-β treatment induced only weak phosphorylation of Smad3L/C at Thr in comparison with pSmad2L/C at Thr. Because Ras-activated JNK signaling caused nuclear translocation of pSmad3L (Supplementary Fig. S3; ref. 17) and linker phosphorylation of Smad3 indirectly blocked its COOH-terminal phosphorylation (Supplementary Fig. S1), TGF-β signaling in the presence of activated Ras could induce COOH-terminal phosphorylation mainly of pSmad2L at Thr^{220} and Ser^{245}.

pSmad2L/C signaling enhances cell invasion by up-regulation of MMP-9. We next assessed whether TGF-β and PDGF treatment induced infiltrative potency in Smad2$^{-/-}$ MEFs expressing Smad2 mutants lacking individual phosphorylation sites (Fig. 2*A*). TGF-β and PDGF treatment additively increased the infiltrative potency of Smad2$^{+/+}$ MEFs (Fig. 2*B*). Forced expression of wild-type (WT*) Smad2 in Smad2$^{-/-}$ MEFs led to recovery of infiltrative potency triggered by TGF-β and/or PDGF stimulation, indicating that Smad2 is essential for the ligand-dependent activities. As expected, Smad2$^{-/-}$ MEFs carrying Smad2(3SA), which lacks COOH-terminal serine residues, showed no invasion in a chamber assay after either TGF-β or PDGF stimulation. Surprisingly, neither TGF-β nor PDGF treatment could induce any infiltrative potency in Smad2 mutants lacking individual phosphorylation sites at Thr^{220}, Ser^{245}, Ser^{250}, or Ser^{255} in the linker region. Taken together, the results indicated that promotion of cell invasion by TGF-β required both complete linker and COOH-terminal phosphorylation of Smad2.

Because MMP-2 and MMP-9 are important in metastasis, we examined whether MMP-2 or MMP-9 is required for TGF-β– or PDGF-induced invasion by Smad2$^{+/+}$ MEFs and Smad2$^{-/-}$ MEFs expressing Smad2WT*. Both basal and ligand-induced invasive activities in the MEFs were inhibited by a MMP-2/MMP-9 inhibitor (Fig. 2*C*) but were less inhibited by a MMP-13 inhibitor (data not shown). TGF-β and/or PDGF treatment to Smad2$^{+/+}$ MEFs did not show induction of MMP-2 expression (data not shown). In addition, because invasion and metastasis of cancer are closely associated with TGF-β–mediated up-regulation of MMP-9 (31), we investigated the effect of linker and/or COOH-terminal

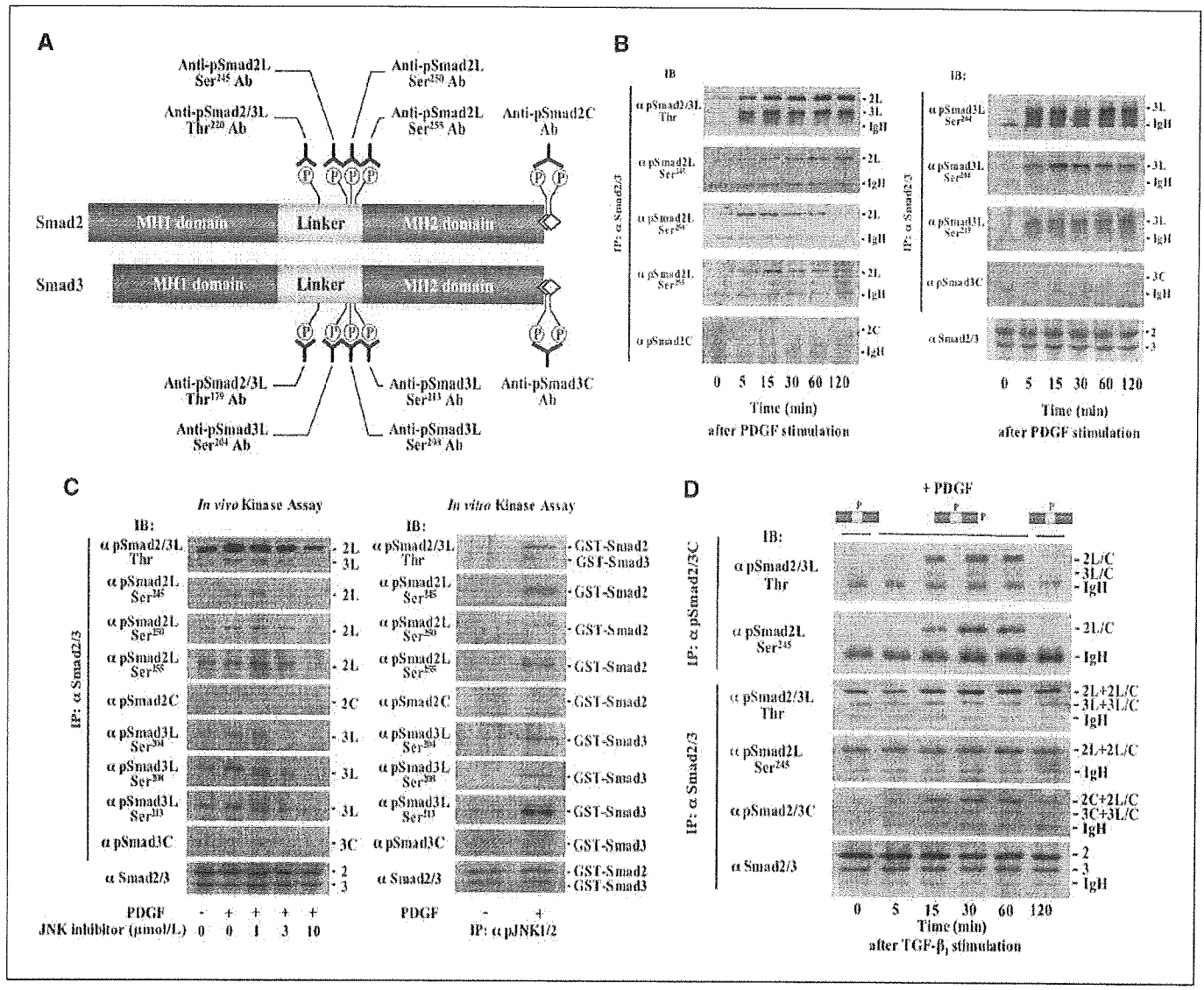

Figure 1. TGF-β signaling converts JNK-dependent pSmad2L into pSmad2L/C. *A*, schematic diagram of phosphorylation sites in Smad2 and Smad3 recognized by antibodies (*Ab*). *B*, serum-derived Smad2$^{+/+}$ MEFs were treated with 400 pmol/L PDGF for the indicated times. Following immunoprecipitation (*IP*) of cell lysates with anti-Smad2/3 antibody, phosphorylation of Smad2 (*left*) and Smad3 (*right*) was analyzed by immunoblotting (*IB*) as indicated. *C*, *left*, serum-deprived Smad2$^{+/+}$ MEFs were pretreated with a JNK inhibitor, SP600125, at the indicated concentration for 2 h before being stimulated for 15 min with 400 pmol/L PDGF. Phosphorylation of Smad2 and Smad3 was analyzed as described above. *Right*, serum-deprived Smad2$^{+/+}$ MEFs were incubated for 15 min with 400 pmol/L PDGF. Cytosolic extracts were immunoprecipitated with anti–phospho-JNK antibody. *In vitro* kinase assays were performed using GST-tagged Smad2 and Smad3 as substrates. Phosphorylation of Smad2/3 was analyzed by immunoblotting as indicated. *D*, serum-deprived Smad2$^{+/+}$ MEFs were pretreated with 400 pmol/L PDGF for 1 h before being stimulated with 200 pmol/L TGF-β_1 for the indicated times. Following immunoprecipitation of nuclear extracts with anti-pSmad2/3C antibody, linker phosphorylation of pSmad2C and pSmad3C was analyzed by immunoblotting using anti-pSmad2/3L (Thr) antibody or anti-pSmad2L (Ser^{245}) antibody.

phosphorylation of Smad2 on induction of MMP-9 protein. Reflecting the invasion profile of the MEFs (Fig. 2*B*), introduction of Smad2WT* in Smad2$^{-/-}$ MEFs led to recovery of ligand-dependent induction of MMP-9 protein. Combined treatment with TGF-β and PDGF of Smad2$^{-/-}$ MEFs expressing Smad2 mutants lacking phosphorylation sites in either the linker region (Smad2EPSM) or the COOH-terminal region [Smad2(3SA)] could not induce MMP-9 protein (Fig. 2*D*). In support of this observation, we determined that TGF-β and PDGF-dependent MMP-9 activity each required both linker and COOH-terminal phosphorylation of Smad2 (data not shown). Collectively, the data showed that TGF-β together with PDGF induced MMP-9–mediated cell invasion through the pSmad2L/C pathway.

Linker phosphorylation of Smad2 requires TβRI-dependent COOH-terminal phosphorylation. We also investigated the kinetics of Smad2/3 phosphorylation in response to TGF-β stimulation. In contrast to the selective linker phosphorylation after PDGF treatment (Fig. 1*B*), TGF-β–dependent phosphorylation of Smad2 and Smad3 occurred not only at all linker sites but also at the COOH-terminal serine residues (Fig. 3*A*). Subcellular localization and linker/COOH-terminal phosphorylation of Smad2$^{-/-}$ MEFs expressing Smad2 mutants lacking phosphorylation sites suggested that nuclear accumulation (Supplementary Fig. S4; ref. 32) and linker phosphorylation of Smad2 (Supplementary Fig. S5) required TGF-β–dependent COOH-terminal phosphorylation. In support of this conclusion, exposure to a TβRI inhibitor

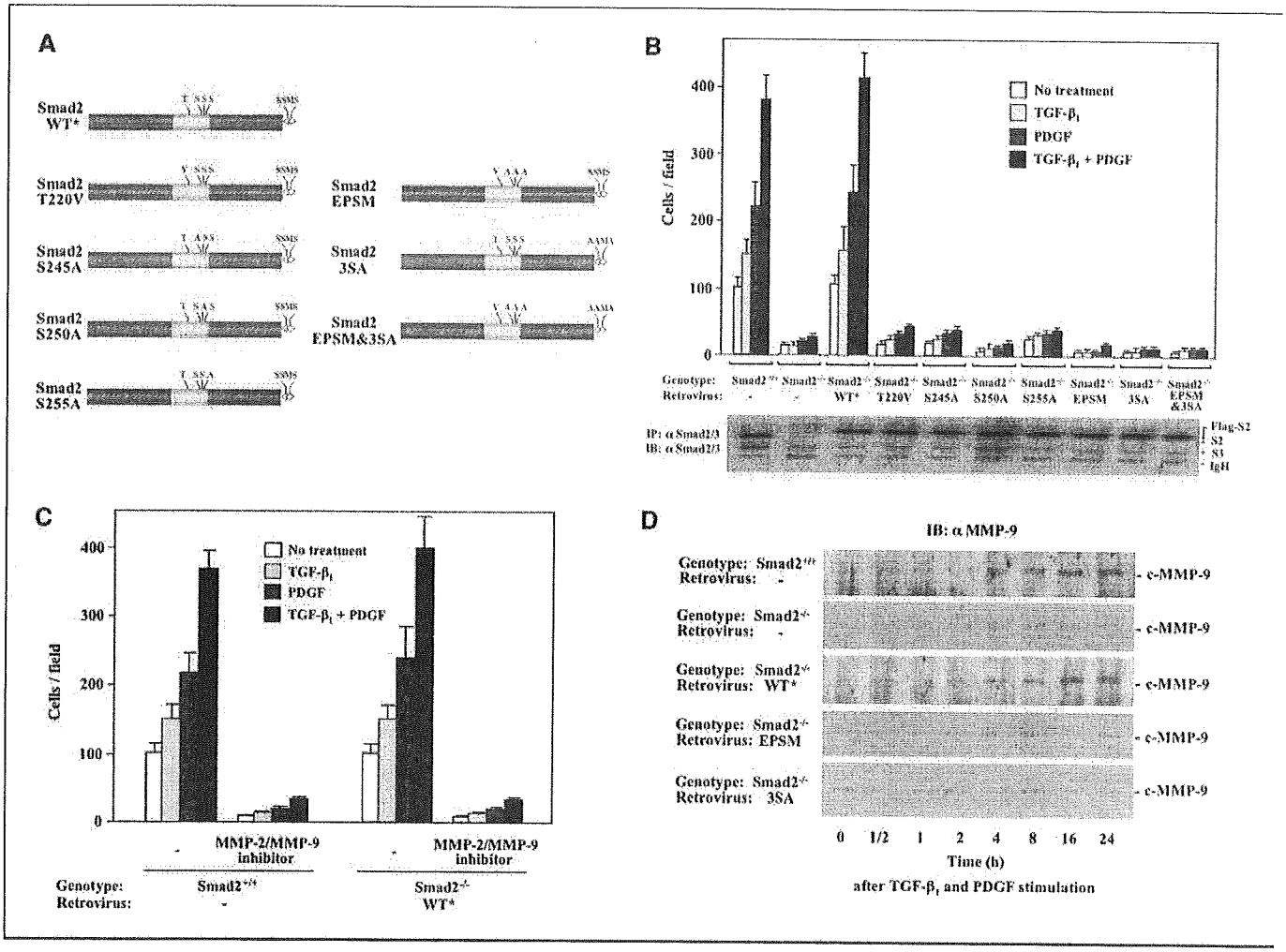

Figure 2. pSmad2L/C signaling enhances cell invasion by up-regulation of MMP-9. *A*, schematic diagram of Smad2 mutants lacking phosphorylation sites in the linker and/or COOH-terminal regions. *B*, serum-derived Smad2$^{+/+}$ MEFs and the infected Smad2$^{-/-}$ MEFs were cultured on Matrigel for 8 h with 200 pmol/L TGF-β_1 and/or 400 pmol/L PDGF. Infiltrating cells were counted. *Columns*, mean (n = 4) from a representative experiment; *bars*, SD. *C*, Matrigel invasion assay for Smad2$^{+/+}$ MEFs and Smad2$^{-/-}$ MEFs expressing Smad2WT* was performed in the absence or presence of a MMP-2/MMP-9 inhibitor (5 μmol/L). *Columns*, mean (n = 4) from a representative experiment; *bars*, SD. *D*, serum-deprived Smad2$^{+/+}$ MEFs and the infected Smad2$^{-/-}$ MEFs were treated with 200 pmol/L TGF-β_1 and 400 pmol/L PDGF for the indicated times. MMP-9 protein was analyzed by immunoblotting using anti–MMP-9 antibody.

SB431542 caused loss of not only COOH-terminal phosphorylation but also linker phosphorylation (Fig. 3*B*).

Nuclear CDK4 converts pSmad2C and pSmad3C into pSmad2L/C and pSmad3L/C. TGF-β induced pSmad2L/C and pSmad3L/C after nuclear translocation of pSmad2C and pSmad3C (Fig. 3*C*; Supplementary Fig. S5). The results indicated that nuclear kinases could phosphorylate linker segments of pSmad2C and pSmad3C. A previous report suggested that CDK4 phosphorylated the linker region of Smad3 (13). Because CDK4 was localized in the nuclei irrespective of whether or not the Smad2$^{+/+}$ MEFs received TGF-β or PDGF treatment (Supplementary Fig. S6), and Thr in Smad2/3L, Ser^{255} in Smad2L, and Ser^{213} in Smad3L served as substrates for CDK4 both *in vivo* and *in vitro* at 90 minutes after TGF-β and PDGF treatment (Fig. 3*D*), we concluded that CDK4 was involved in linker phosphorylation of pSmad2C and pSmad3C in the nuclei of the MEF.

Stimulation of cell growth by up-regulating c-Myc oncoprotein requires TGF-β–mediated linker phosphorylation. We further investigated whether linker phosphorylation affected growth of the MEF. As shown in Fig. 4*A* and *B*, expression of Smad2(3SA) in Smad2$^{-/-}$ MEFs did not influence growth. However, the T220V, S245A, and S255A mutants showed suppression of growth in response to TGF-β. Smad2EPSM showed the most prominent TGF-β–mediated growth inhibition. These results indicated that Smad2 phosphorylation at Thr^{220}, Ser^{245}, and Ser^{255} collectively blocked the growth-inhibitory effect of TGF-β, although Smad2 mutants lacking individual phosphorylation sites in the linker region showed weaker suppression of growth in response to TGF-β than corresponding Smad3 mutants (Supplementary Fig. S7; ref. 13).

TGF-β inhibits cell growth through Smad-mediated transcriptional regulation of critical regulators of the cell cycle (9). The first direct transcriptional target of the TGF-β pathway that explains how this cytokine inhibits cell proliferation is c-Myc (33), whose expression in Smad2$^{+/+}$ MEFs and Smad2$^{-/-}$ MEFs expressing Smad2WT* were initially repressed by TGF-β (Fig. 4*C* and *D*); later, however, TGF-β signaling underwent a complete change to induce c-Myc protein. In contrast, TGF-β persistently inhibited c-Myc expression and growth in Smad2$^{-/-}$ MEFs expressing Smad2EPSM. Because expression of cyclin D1 in Smad2EPSM MEFs appeared at

1 h after addition of TGF-β, and remained high at 24 hours (Supplementary Fig. S8), the cyclin D1-CDK4 complex was active in the cells (34). Taken together, TGF-β inhibited cell growth by down-regulating c-Myc transcription through the pSmad2C and pSmad3C pathway; TGF-β signaling, in turn, enhanced cell growth by up-regulating c-Myc after the additional phosphorylation of pSmad2C and pSmad3C at their linker regions.

Malignant signaling by pSmad2L/C and pSmad3L/C in human metastatic colorectal cancer. We finally investigated whether perturbation of TGF-β signaling involved linker phosphorylation of Smad2 and Smad3 in 20 human metastatic colorectal tumors (Supplementary Table S1). Because perturbation of TGF-β signaling results from mutations that inactivate TGF-β receptors or Smad signal transducers in a portion of gastrointestinal cancers (9), we analyzed mutations of these genes in the human metastatic colorectal cancer samples. MH2 region sequencing in *Smad4* gene revealed a G/A substitution at codon 361 in one cancer (Arg to His; patient 5 in Supplementary Table S1), but no mutations were found in *TβRII* or *Smad2* genes from any colorectal tumor samples.

Figure 5*A* shows the distribution of TGF-β_1 and phosphorylated Smad2/3 in a metastatic colon tumor and nearby uninvolved normal liver tissue from patient 1 in Supplementary Table S1. Immunostaining for TGF-β_1 showed diffuse cytoplasmic positivity

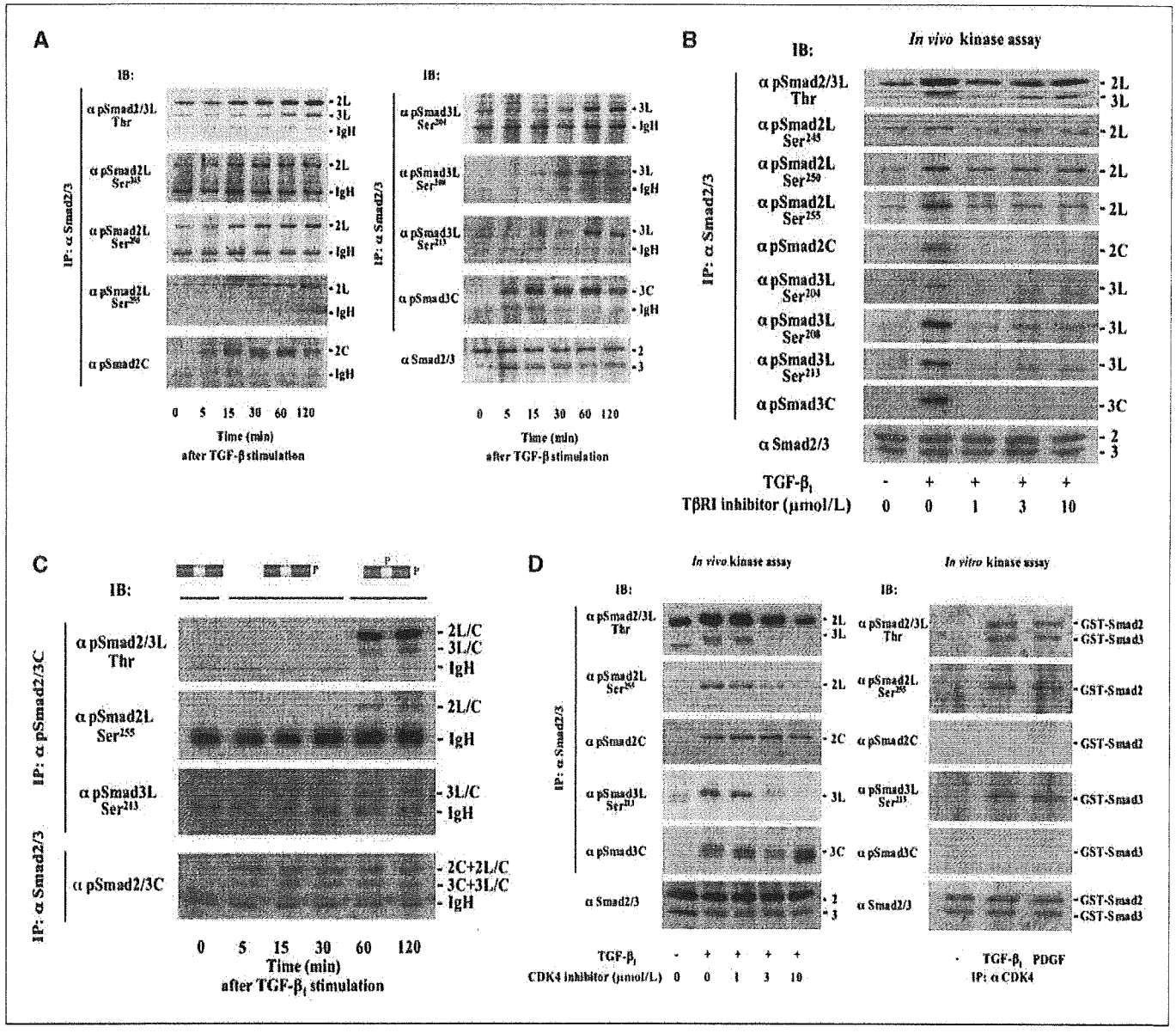

Figure 3. Nuclear CDK4 converts pSmad2C and pSmad3C into pSmad2L/C and pSmad3L/C. *A*, serum-deprived Smad2$^{+/+}$ MEFs were incubated with TGF-β for the indicated times. Following immunoprecipitation of cell lysates with anti-Smad2/3 antibody, domain-specific phosphorylation was analyzed by immunoblotting using anti–phospho-Smad2 antibodies (*left*) and anti–phospho-Smad3 antibodies (*right*). *B*, serum-deprived Smad2$^{+/+}$ MEFs were pretreated with a TβRI inhibitor SB431542 at the indicated concentration for 2 h before being stimulated for 1 h with 200 pmol/L TGF-β_1. Phosphorylation of Smad2 and Smad3 was analyzed as described above. *C*, serum-deprived Smad2$^{+/+}$ MEFs were incubated with 200 pmol/L TGF-β_1 for the indicated times. Following immunoprecipitation of nuclear extracts with anti-pSmad2/3C antibody, phosphorylation at the indicated linker sites was analyzed by immunoblotting using anti–phospho-Smad2/3L antibodies. *D, left*, serum-deprived Smad2$^{+/+}$ MEFs were pretreated with a CDK4 inhibitor as described above. *Right*, serum-deprived Smad2$^{+/+}$ MEFs were incubated for 90 min with 200 pmol/L TGF-β_1 or 400 pmol/L PDGF. Nuclear extracts were immunoprecipitated with anti-CDK4 antibody. *In vitro* kinase assay was performed as described above.

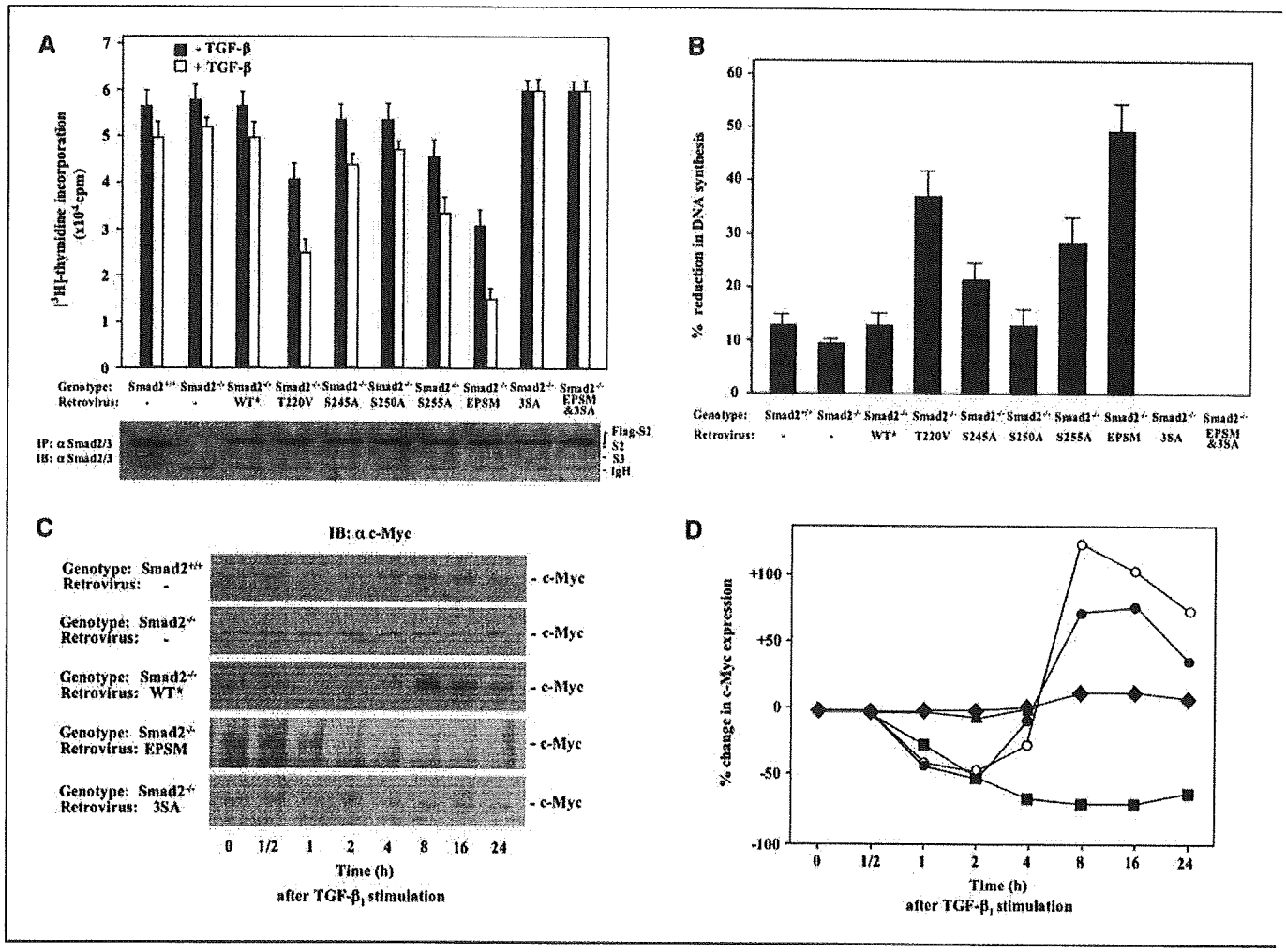

Figure 4. Stimulation of cell growth by up-regulating c-Myc oncoprotein requires TGF-β–mediated Smad2 linker phosphorylation. *A*, serum-deprived Smad2$^{+/+}$ MEFs and the infected Smad2$^{-/-}$ MEFs were compared in [^{3}H]thymidine incorporation assay in the absence (*filled columns*) and in the presence (*open columns*) of TGF-β. *Columns*, mean (n = 4) from a representative experiment; *bars*, SD. *B*, percentage reduction of [^{3}H]thymidine incorporation of Smad2$^{+/+}$ MEFs and the infected Smad2$^{-/-}$ MEF. MEFs were treated with TGF-β and processed as in *A*. Acid-insoluble [^{3}H]thymidine was counted and compared with that incorporated by cells that had not been exposed to TGF-β$_1$ treatment. Each T220V, S245A, and S255A mutant showed greater enhancement of the growth-inhibitory effect of TGF-β than Smad2WT* or 3SA mutant. Smad2EPSM showed the most enhancement. *C*, serum-deprived Smad2$^{+/+}$ MEFs and the infected Smad2$^{-/-}$ MEFs were incubated with 200 pmol/L TGF-β$_1$ for the indicated times. Expression of c-Myc was analyzed by immunoblotting using anti–c-Myc antibody. *D*, graphic analyses of the immunoblots yielded the ratio of TGF-β–inducible c-Myc expression to that without TGF-β treatment. Percentage increase/reduction in intensity of c-Myc bands after TGF-β treatment of MEFs was calculated relative to the intensity without TGF-β treatment. In Smad2$^{+/+}$ MEFs (●) and Smad2$^{-/-}$ MEFs expressing Smad2WT* (○), c-Myc was initially repressed by TGF-β. Later, TGF-β signaling underwent a complete change favoring induction of c-Myc protein. In contrast, TGF-β persistently inhibited c-Myc production in Smad2$^{-/-}$ MEFs expressing Smad2EPSM (■). Smad2$^{-/-}$ MEFs expressing Smad3SA (▲) maintained basal c-Myc expression, similarly to parental Smad2$^{-/-}$ MEFs (◆).

throughout the tumor specimen (Fig. 5*A, top left of α TGF-β$_1$ panel*). The degree of Smad2C phosphorylation in the tumor was almost the same as that in normal liver, and pSmad2C was distributed evenly in the nuclei of tumor cells (Fig. 5*A, top left compared with bottom right of α pSmad2C panel*). Although Smad3 was slightly phosphorylated at the COOH-terminal region in normal liver cells, Smad3C was highly phosphorylated in the nuclei of the tumor cells (Fig. 5*A, top left compared with bottom right of α pSmad3C panel*). Both Smad2L and Smad3L showed little phosphorylation in normal liver (Fig. 5*A, bottom right of α pSmad2/3L Thr, αpSmad2L Ser^{255}, and α pSmad3L Ser^{213} panels*). In contrast, Smad2 and Smad3 in the tumor were highly phosphorylated at the linker regions, and linker-phosphorylated Smad2 and Smad3 were localized in the nuclei of tumor cells (Fig. 5*A, top left of α pSmad2/3L Thr, αpSmad2L Ser^{255}, and α pSmad3L Ser^{213} panels*). In particular, the invasion fronts of two metastatic colon tumors (patients 10 and 16 in Supplementary Table S1) showed strong nuclear signals for pSmad2/3L (Thr; Fig. 5*B*).

Domain-specific phospho-Smad2/3 immunoblotting of tissue extracts from the same patient showed that Smad2 and Smad3 in the tumor were highly phosphorylated at both linker and COOH-terminal regions (Fig. 5*C, top left*). Phospho-Smad2/3L immunoblotting of pSmad2/3C immunoprecipitates from nuclear extracts showed that pSmad2L/C and pSmad3L/C were localized in cell nuclei of TGF-β–producing metastatic colon tumor (Fig. 5*C, top right*). Taken together with *in vitro* experiments, aberrant phosphorylation of Smad2L/C and Smad3L/C could lead to uncontrollable tumor growth and invasion. *In vitro* kinase assay confirmed that cytosolic JNK and nuclear CDK4 obtained from the tumor tissue could phosphorylate Smad2 or Smad3 at their linker regions (Fig. 5*C,*

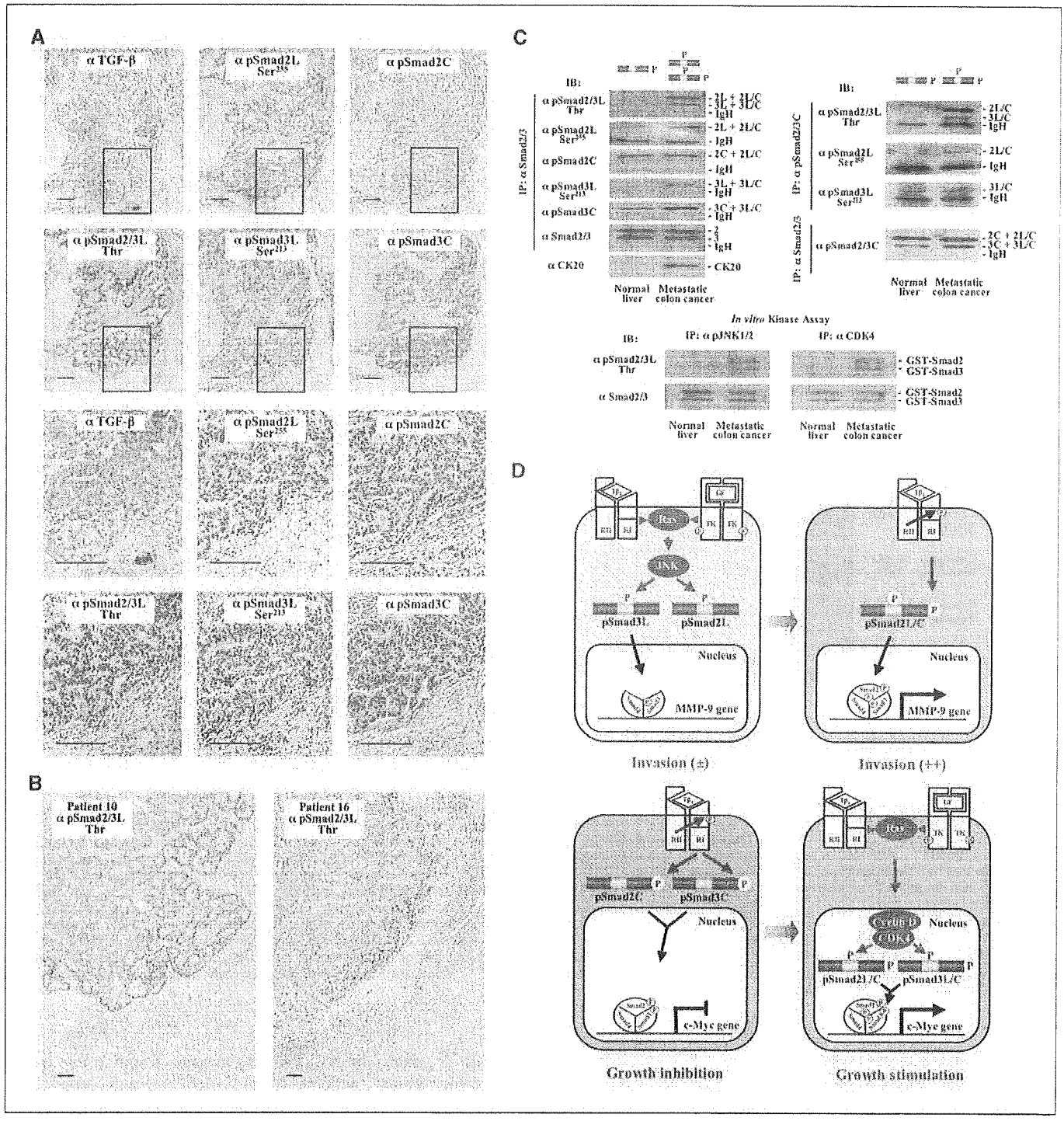

Figure 5. Malignant signaling by pSmad2L/C and pSmad3L/C in human metastatic colorectal cancer. *A,* formalin-fixed, paraffin-embedded sections of metastatic cancer tissue and uninvolved normal liver from patient 1 in Supplementary Table S1 were stained as indicated. All sections were counterstained with hematoxylin (*blue*). Brown staining indicates specific antibody reactivity. *Bar,* 50 μm. The lower six small panels show higher magnification of the boxed areas in the corresponding panels above. *B,* formalin-fixed, paraffin-embedded sections of metastatic cancer tissues and uninvolved livers from patients 10 and 16 in Supplementary Table S1 were stained with an anti-pSmad2/3L (Thr) antibody. *C, top left,* cell extracts of cancer tissue and uninvolved normal liver from the same patient were subjected to anti-Smad2/3 immunoprecipitation and were immunoblotted as indicated. Cytokeratin 20 (CK20) as the marker in tumors metastasized from colon was analyzed by immunoblotting (*bottom*). *Top right,* nuclear extracts of cancer tissue and uninvolved normal liver from this patient were subjected to anti-pSmad2/3C immunoprecipitation and then were immunoblotted as indicated; *bottom,* cytosolic and nuclear extracts of cancer tissue and uninvolved normal liver tissue from the patient were immunoprecipitated with anti–phospho-JNK antibody and anti-CDK4 antibody, respectively. After *in vitro* kinase assay, phosphorylation of Smad2L and Smad3L was analyzed by immunoblotting using anti-pSmad2/3L (Thr) antibody. *D, top,* PDGF activates JNK, thereby phosphorylating Smad2L and Smad3L. After COOH-terminal phosphorylation of cytoplasmic pSmad2L by TβRI, pSmad2L/C undergoes translocation to the nucleus, where it interacts with pSmad3L (25). Consequently, the Smads complex stimulates MMP-9 transcription and cell invasion. *Bottom,* TGF-β inhibits cell growth by down-regulating c-Myc oncoprotein through the pSmad2C and pSmad3C pathway; TGF-β signaling, in turn, enhances cell growth by up-regulating c-Myc through the CDK4-dependent pSmad2L/C and pSmad3L/C pathway.

bottom). These results pointed to additive requirement of JNK and CDK4 activities for the formation of pSmad2L/C and pSmad3L/C in advanced stages of human colorectal cancer.

Discussion

Our results provide a new view of TβRI and Ras-associated kinases cooperating to promote cancer progression by up-regulating invasion- and growth-related proteins. Thus, pSmad2L/C and pSmad3L/C can mediate the malignant signaling that allows human metastatic cancer to adopt more invasive and proliferative properties required for progression (Fig. 5*D*).

In contrast to the finding of COOH-terminal phosphorylation of Smad2 and Smad3 in almost all cell types and tissues (10), timing, duration, extent, and functional implications of their linker phosphorylation depend on cell type and differ by the stage of cancer progression. Therefore, the role of linker phosphorylation in COOH-terminal phosphorylation has been controversial with varying data, suggesting that Ras-mediated linker phosphorylation either inhibits (11, 17, 19–22) or enhances (36–46) events downstream of TβRI. To explain the disparate findings, we analyzed phospho-Smad2/3 profiles in a single model of colon cancer using a pair of cell lines, human normal intestinal epithelial cells, and human colon cancer cells, to validate our hypothesis that linker phosphorylation changes during cancer progression (Fig. 6).

First, involvement of different kinases may explain for differing outcomes among various cell types and contexts. Normal epithelial cells generally show rapid phosphorylation at Smad2/3L in response to TGF-β (Fig. 6*A*; ref. 12). The kinases seem to act before Smad2 or Smad3 reaches the nucleus. Both JNK and ERK are localized in the cytoplasm and directly phosphorylate the linker regions, creating pSmad2L and pSmad3L (11, 12, 42). In contrast, TGF-β–induced linker phosphorylation in established mesenchymal cells such as MEFs is very slow. Mesenchymal cells show TGF-β–inducible linker phosphorylation after nuclear translocation of pSmad2/3C (Fig. 6*B*; present work). As epithelial cells are transformed into cancer cells, they come to exhibit strong constitutive linker phosphorylation (Fig. 6*C*; ref. 17). Nuclear CDK4, together with cytoplasmic JNK, converts a tumor-suppressive pSmad2/3C signal into malignant characteristics. Thus, TGF-β signaling confers a selective advantage on cancer cells by shifting from pSmad2C and pSmad3C pathway characteristic of mature epithelial cells to the pSmad2L/C and pSmad3L/C pathway, which is more characteristic of the state of flux shown by the activated mesenchymal cells. Loss of epithelial homeostasis and acquisition of a migratory, mesenchymal phenotype are essential for invasion in later stages of human cancer (47). In particular, tumors with features characteristic of epithelial-mesenchymal transition have been found at invasion fronts, where strong phosphorylation of Smad2L/C and Smad3L/C was observed (Fig. 5*B*; ref. 2).

The second possibility involves differential duration of linker phosphorylation among various cell types. Although linker phosphorylation is transient after TGF-β treatment of normal epithelial cells (Fig. 6*A*; ref. 12), TGF-β–inducible phosphorylation is generally persistent in various mesenchymal cells (Fig. 6*B*; present work). Moreover, constitutive linker phosphorylation is found in almost all types of cancer cells, including Ras-transformed cells and cancer tissues (Fig. 6*C*; refs. 17, 19–22). Phosphorylation of many transcription factors is controlled by a dynamic interplay between kinases and phosphatases. Several lines of evidences have identified small COOH-terminal domain phosphatase (SCP1-3) as Smad2/3 linker–specific phosphatases (15, 48). SCP1-3 dephosphorylate

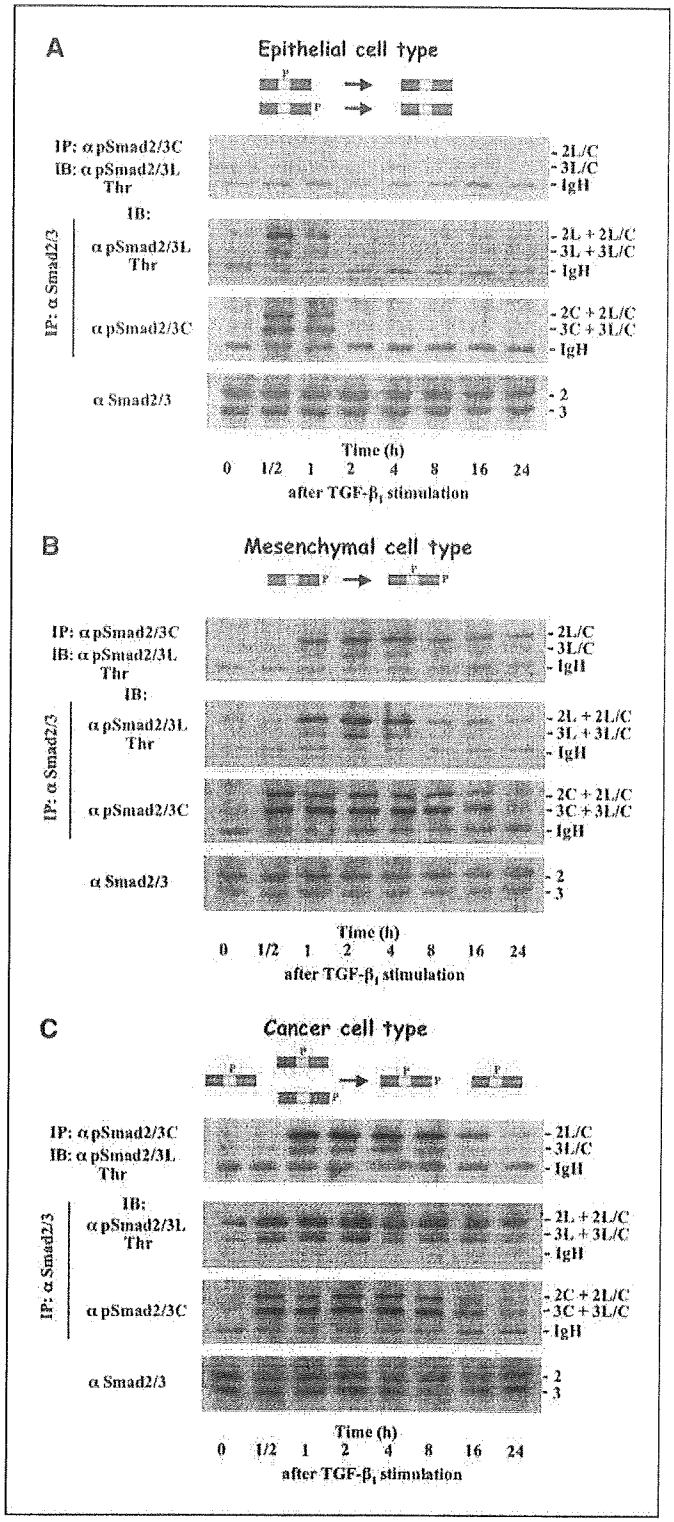

Figure 6. Timing, duration, and extent of linker phosphorylation differ among normal intestinal epithelial cells, mesenchymal cells, and colon cancer cells, whereas COOH-terminal phosphorylation is a common feature. Serum-deprived human normal intestinal epithelial cells (*A*), MEFs (*B*), and human colon cancer cells (*C*) were incubated with 200 pmol/L TGF-β_1 for the indicated times. Immunoprecipitation and immunoblotting were performed as described above.

Ser^{245}, Ser^{250}, and Ser^{255} sites in Smad2L or Ser^{204}, Ser^{208}, and Ser^{213} sites in Smad3L (48). Accordingly, SCP1-3 might dephosphorylate the Ser phosphorylation in normal epithelial cells. Linker phosphorylation in mesenchymal cells and cancer cells might show resistance to the phosphatases. Alternatively, these cells may not be able to induce or activate the relevant phosphatases. One should note that phosphorylation at Thr^{220} in Smad2L and at Thr^{179} in Smad3L could not be dephosphorylated by SCP1-3, although several kinases (CDK4, JNK, and ERK) could phosphorylate the threonine residues (11, 13, 17, 48). In this regard, our current data showed that metastatic tumors were constitutively transmitting malignant signals through the phosphorylated threonine residues (Fig. 5).

The final possibility to consider involves the differences in effect of TGF-β on receptor tyrosine kinase (RTK)–mediated signaling between epithelial and mesenchymal cells. TGF-β and RTKs are known to exert mutually antagonistic effects on cell cycle control and apoptosis in normal epithelial cells (49, 50). Because linker phosphorylation of Smad3 indirectly inhibits its COOH-terminal phosphorylation (Supplementary Fig. S1), the proliferative effect mediated through the RTK-dependent pSmad3L pathway antagonizes TGF-β signaling through the cytostatic pSmad3C pathway in normal epithelial cells (14). In normal epithelial cells, pSmad2L/C and pSmad3L/C rarely exist either *in vitro* or *in vivo* (Fig. 6*A*; refs. 20–22). In contrast, TGF-β and RTKs synergistically promote growth and invasion of mesenchymal cells (1). Blocking either linker or COOH-terminal phosphorylation of Smad2 abrogated the synergistic responses of MEFs to TGF-β and PDGF (Figs. 2 and 4), indicating involvement of pSmad2L/C in this synergistic response of mesenchymal cells.

Thus far, we have investigated the phosphoisoforms of Smad2 and Smad3 in >2,000 human cancer tissue specimens, finding that their distribution correlates well with the pathologic features. In mature epithelial cells, pSmad2C and pSmad3C are predominantly located in the nuclei. In contrast, pSmad2L/C and pSmad3L/C show nuclear localization at invasion fronts of several types of advanced cancers with distant metastasis. Restoration in cancer of the lost tumor-suppressive function observed in normal epithelial cells, together with disruption of the fundamental signaling pathways that enable tumors to grow and invade, would represent an elegant therapeutic approach. Accordingly, we have reason to hope that pharmacologic inhibition of linker phosphorylation can suppress progression of human advanced cancer by causing a shift from malignant to tumor-suppressive TGF-β signaling (17, 22). Additionally, when evaluating effectiveness of targeted therapies for human cancer, domain-specific phosphorylation of Smad2 and Smad3 should be useful biomarkers likely to correlate with patient responses (22).

Disclosure of Potential Conflicts of Interest

No potential conflicts of interest were disclosed.

Acknowledgments

Received 11/6/08; revised 3/19/09; accepted 5/6/09; published OnlineFirst 6/16/09.

Grant support: Grant-in-Aid for scientific research from the Ministry of Education, Science and Culture of Japan.

The costs of publication of this article were defrayed in part by the payment of page charges. This article must therefore be hereby marked *advertisement* in accordance with 18 U.S.C. Section 1734 solely to indicate this fact.

We thank Dr. R. Derynck (University of California at San Francisco) for providing cDNAs encoding human Smad2 and Smad3; Drs. C. Stuelten and A. Roberts (National Cancer Institute) for providing $Smad2^{-/-}$ MEFs; Drs. K. Kobayashi and K. Yokote (Chiba University) for providing $Smad3^{-/-}$ mice; and N. Ohira for assistance with immunoblotting.

References

1. Roberts AB, Sporn MB. The transforming growth factor-βs. In: Sporn MB, Roberts AB, editors. Peptide growth factors and their receptors. Berlin: Springer-Verlag; 1990. p. 419–72.
2. Akhurst RJ. TGF-β signaling in health and disease. Nat Genet 2004;36:790–2.
3. Wakefield LM, Roberts AB. TGF-β signaling: positive and negative effects on tumorigenesis. Curr Opin Genet Dev 2002;12:22–9.
4. Oft M, Peli J, Rudaz C, Schwarz H, Beug H, Reichmann E. TGF-β1 and Ha-Ras collaborate in modulating the phenotypic plasticity and invasiveness of epithelial tumor cells. Genes Dev 1996;10:2462–77.
5. Tian F, DaCosta Byfield S, Parks WT, et al. Reduction in Smad2/3 signaling enhances tumorigenesis but suppresses metastasis of breast cancer cell lines. Cancer Res 2003;63:8284–92.
6. Arteaga CL. Inhibition of TGF-β signaling in cancer therapy. Curr Opin Genet Dev 2006;16:30–7.
7. Matsuyama S, Iwadate M, Kondo M, et al. SB-431542 and Gleevec inhibit transforming growth factor-β-induced proliferation of human osteosarcoma cells. Cancer Res 2003;63:7791–8.
8. Heldin CH, Miyazono K, ten Dijke P. TGF-β signaling from cell membrane to nucleus through SMAD proteins. Nature 1997;390:465–71.
9. Massagué J. TGF-β signal transduction. Annu Rev Biochem 1998;67:753–91.
10. Wrana JL. Crossing Smads. Sci STKE 2000;23:re1.
11. Kretzschmar M, Doody J, Timokhina I, Massagué J. A mechanism of repression of TGF-β/Smad signaling by oncogenic Ras. Genes Dev 1999;13:804–16.
12. Mori S, Matsuzaki K, Yoshida K, et al. TGF-β and HGF transmit the signals through JNK-dependent Smad2/3 phosphorylation at the linker regions. Oncogene 2004;23:416–29.
13. Matsuura I, Denissova NG, Wang G, He D, Long J, Liu F. Cyclin-dependent kinases regulate the antiproliferative function of Smads. Nature 2004;430:226–31.
14. Matsuzaki K. Smad3 phosphoisoform-mediated signaling during sporadic human colorectal carcinogenesis. Histol Histopathol 2006;21:645–62.
15. Sapkota G, Knockaert M, Alarcón C, Montalvo E, Brivanlou AH, Massagué J. Dephosphorylation of the linker regions of Smad1 and Smad2/3 by small C-terminal domain phosphatases has distinct outcomes for bone morphogenetic protein and transforming growth factor-β pathways. J Biol Chem 2006;281:40412–9.
16. Derynck R, Zhang YE. Smad-dependent and Smad-independent pathways in TGF-β family signaling. Nature 2003;425:577–84.
17. Sekimoto G, Matsuzaki K, Yoshida K, et al. Reversible Smad-dependent signaling between tumor suppression and oncogenesis. Cancer Res 2007;67:5090–6.
18. Arany PR, Rane SG, Roberts AB. Smad3 deficiency inhibits v-ras-induced transformation by suppression of JNK MAPK signaling and increased farnesyl transferase inhibition. Oncogene 2008;27:2507–12.
19. Yamagata H, Matsuzaki K, Mori S, et al. Acceleration of Smad2 and Smad3 phosphorylation via c-Jun NH(2)-terminal kinase during human colorectal carcinogenesis. Cancer Res 2005;65:157–65.
20. Matsuzaki K, Murata M, Yoshida K, et al. Chronic inflammation associated with hepatitis C virus infection perturbs hepatic transforming growth factor β signaling, promoting cirrhosis and hepatocellular carcinoma. Hepatology 2007;46:48–57.
21. Murata M, Matsuzaki K, Yoshida K, et al. Hepatitis B virus X protein shifts human hepatic TGF-β signaling from tumor-suppression to oncogenesis in early chronic hepatitis B. Hepatology 2009;49:1203–17.
22. Nagata H, Hatano E, Tada M, et al. Inhibition of c-Jun NH2-terminal kinase switches Smad3 signaling from oncogenesis to tumor-suppression in rat hepatocellular carcinoma. Hepatology. In press, 2009.
23. Kobayashi K, Yokote K, Fujimoto M, et al. Targeted disruption of TGF-β-Smad3 signaling leads to enhanced neointimal hyperplasia with diminished matrix deposition in response to vascular injury. Circ Res 2005;96:904–12.
24. Ilyas M, Efstathiou JA, Straub J, Kim HC, Bodmer WF. Transforming growth factor β stimulation of colorectal cancer cell lines: type II receptor bypass and changes in adhesion molecule expression. Proc Natl Acad Sci U S A 1999;96:3087–91.
25. Furukawa F, Matsuzaki K, Mori S, et al. p38 MAPK mediates fibrogenic signal through Smad3 phosphorylation in rat myofibroblasts. Hepatology 2003;38:879–89.
26. Hutter RVP, Sobin LH. A universal staining system for cancer of the colon and rectum. Arch Pathol Lab Med 1986;110:367–8.
27. Markowitz S, Wang J, Myeroff L, et al. Inactivation of the type II TGF-β receptor in colon cancer cells with microsatellite instability. Science 1995;268:1336–8.
28. Grady WM, Myeroff LL, Swinler SE, et al. Mutational inactivation of transforming growth factor β receptor type II in microsatellite stable colon cancers. Cancer Res 1999;59:320–4.
29. Riggins GJ, Thiagalingam S, Rozenblum E, et al. Mad-related genes in the human. Nat Genet 1996;13:347–9.
30. Takagi Y, Kohmura H, Futamura M, et al. Somatic alterations of the DPC4 gene in human colorectal cancers *in vivo*. Gastroenterology 1996;111:1369–72.
31. Safina A, Vandette E, Bakin AV. ALK5 promotes

tumor angiogenesis by upregulating matrix metalloproteinase-9 in tumor cells. Oncogene 2007;26:2407–22.
32. Macias-Silva M, Abdollah S, Hoodless PA, Pirone R, Attisano L, Wrana JL. MADR2 is a substrate of the TGF β receptor and its phosphorylation is required for nuclear accumulation and signaling. Cell 1996;87:1215–24.
33. Chen CR, Kang Y, Siegel PM, Massagué J. E2F4/5 and p107 as Smad cofactors linking the TGF β receptor to c-myc repression. Cell 2002;110:19–32.
34. Matsushime H, Ewen ME, Strom DK, et al. Identification and properties of an atypical catalytic subunit (p34PSK-J3/cdk4) for mammalian D type G1 cyclins. Cell 1992;71:323–34.
35. Wicks SJ, Lui S, Abdel-Wahab N, Mason RM, Chantry A. Inactivation of smad-transforming growth factor β signaling by Ca(2+)-calmodulin-dependent protein kinase II. Mol Cell Biol 2000;20:8103–11.
36. de Caestecker MP, Parks WT, Frank CJ, et al. Smad2 transduces common signals from receptor serine-threonine and tyrosine kinases. Genes Dev 1998;12:1587–92.
37. Engel ME, McDonnell MA, Law BK, Moses HL. Interdependent SMAD and JNK signaling in transforming growth factor-β-mediated transcription. J Biol Chem 1999;274:37413–20.
38. Brown JD, DiChiara MR, Anderson KR, Gimbrone MA, Topper JN. MEKK-1, a component of the stress (stress-activated protein kinase/c-Jun N-terminal kinase) pathway, can selectively activate Smad2-mediated transcriptional activation in endothelial cells. J Biol Chem 1999;274:8797–805.
39. Yue J, Mulder KM. Requirement of Ras/MAPK pathway activation by transforming growth factor β for transforming growth factor β1 production in a Smad-dependent pathway. J Biol Chem 2000;275:30765–73.
40. Funaba M, Zimmerman CM, Mathews LS. Modulation of Smad2-mediated signaling by extracellular signal-regulated kinase. J Biol Chem 2002;277:41361–8.
41. Janda E, Lehmann K, Killisch I, et al. Ras and TGF-β cooperatively regulate epithelial cell plasticity and metastasis: dissection of Ras signaling pathways. J Cell Biol 2002;156:299–313.
42. Hayashida T, de Caestecker M, Schnaper HW. Cross-talk between ERK MAP kinase and Smad signaling pathways enhances TGF-β-dependent responses in human mesangial cells. FASEB J 2003;17:1576–8.
43. Javelaud D, Mauviel A. Crosstalk mechanisms between the mitogen-activated protein kinase pathways and Smad signaling downstream of TGF-β: implications for carcinogenesis. Oncogene 2005;24:5742–50.
44. Stuelten CH, DaCosta Byfield S, Arany PR, Karpova TS, Stetler-Stevenson WG, Roberts AB. Breast cancer cells induce stromal fibroblasts to express MMP-9 via secretion of TNF-α and TGF-β. J Cell Sci 2005;118:2143–53.
45. Gotzmann J, Fischer AN, Zojer M, et al. A crucial function of PDGF in TGF-β-mediated cancer progression of hepatocytes. Oncogene 2006;25:3170–85.
46. Suzuki K, Wilkes MC, Garamszegi N, Edens M, Leof EB. Transforming growth factor β signaling via Ras in mesenchymal cells requires p21-activated kinase 2 for extracellular signal-regulated kinase-dependent transcriptional responses. Cancer Res 2007;67:3673–82.
47. Derynck R, Akhurst RJ. Differentiation plasticity regulated by TGF-β family proteins in development and disease. Nat Cell Biol 2007;9:1000–4.
48. Wrighton KH, Willis D, Long J, Liu F, Lin X, Feng XH. Small C-terminal domain phosphatases dephosphorylate the regulatory linker regions of Smad2 and Smad3 to enhance transforming growth factor-β signaling. J Biol Chem 2006;281:38365–75.
49. Moses HL, Yang EY, Pietenpol JA. TGF-β stimulation and inhibition of cell proliferation: new mechanistic insights. Cell 1990;63:245–7.
50. Pardali K, Moustakas A. Actions of TGF-β as tumor suppressor and pro-metastatic factor in human cancer. Biochim Biophys Acta 2007;1775:21–62.

Human Neutrophil Peptides 1-3 Are Useful Biomarkers in Patients with Active Ulcerative Colitis

Shuji Kanmura, MD, Hirofumi Uto, MD,* Masatsugu Numata, MD,† Shinichi Hashimoto, MD,* Akihiro Moriuchi, MD,* Hiroshi Fujita, MD,* Makoto Oketani, MD,* Akio Ido, MD,* Mayumi Kodama, MD,‡ Hidehisa Ohi, MD,§ and Hirohito Tsubouchi, MD,**

Background: A specific useful biomarker for diagnosing ulcerative colitis (UC) has not yet been described. This study employed proteomics to identify serum protein biomarkers for UC.

Methods: Ninety-four blood samples were isolated from patients and controls (including 48 UC, 22 Crohn's disease [CD], 5 colorectal cancer, and 6 infectious colitis patients and 13 healthy subjects). Serum samples were analyzed using the SELDI-TOF/MS ProteinChip system. After applying the samples to ProteinChip arrays, we assessed differences in the proteomes using Ciphergen ProteinChip software and identified candidate proteins, which were then characterized in immunoassays.

Results: Preliminary analysis using the ProteinChip system revealed significant peak-intensity differences for 27 serum proteins between 11 patients with UC and 7 healthy subjects. Among these proteins, 3 proteins (with mass/charge ratios of approximately 3400) were identified as human neutrophil peptides 1–3 (HNP 1–3). The presence of HNP 1–3 in the patient sera was confirmed using immunoassays. Enzyme-linked immunosorbent assays demonstrated that the mean plasma concentration of HNP 1–3 was significantly higher in patients with active UC (n = 28) than in patients whose UC was in remission (n = 20) or patients with CD (n = 22), infectious colitis, or healthy subjects, and tended to be higher than in patients with colon cancer. In addition, the plasma concentration of HNP 1–3 in patients that responded to corticosteroids-based therapy decreased after treatment, whereas it was not changed in nonresponders.

Conclusions: HNP 1–3 is a novel biomarker that may be useful for diagnosing patients with active UC and predicting treatment outcomes.

(Inflamm Bowel Dis 2009;15:909–917)

Key Words: biomarkers, inflammatory bowel disease, ulcerative colitis, human neutrophil peptides 1–3, SELDI-TOF/MS, proteomics

Genetic and environmental factors contribute to the disease process of inflammatory bowel disease (IBD), including ulcerative colitis (UC).[1,2] The presence of active inflammation of the gut in patients with UC is associated with an acute-phase reaction and the migration of leukocytes to the gut. This, in turn, promotes the production of a large number of proteins.[3] Determination of inflammatory activity is important for the comprehensive assessment of patients with UC and for the tailoring of therapy.[4] Many clinical activity indices are used to stratify patients with UC. For example, the UC Disease Activity Index (UCDAI)[5] is a widely used measure of clinical parameters of disease activity. These indices, however, only provide indirect assessments of disease activity. Whereas albumin, hemoglobin, the erythrocyte sedimentation rate (ESR), and acute-phase protein levels are commonly used biological parameters for assessing UC, there are no accurate markers to assess the inflammatory activity observed with histopathologic or endoscopic analyses.[6]

Proteomic array technology, in which a ProteinChip system is coupled with surface-enhanced laser desorption ionization/time-of-flight/mass spectrometry (SELDI-TOF/MS) for the profiling of serum or plasma, is a powerful tool that allows the identification of new biomarkers for malignant tumors and autoimmune diseases.[7,8] This technology is a rapid and sensitive technique, in which the detected peak intensities for some proteins correlate with concentrations determined using enzyme-linked immunosorbent assay (ELISA). Novel blood biomarkers which are identified by this proteomics, may provide clinicians with more accurate parameters to assess inflammatory activity in UC.

Received for publication October 29, 2008; Accepted November 14, 2008.

From the *Digestive Disease and Life-style Related Disease Health Research, Human and Environmental Sciences, Kagoshima University Graduate School of Medical and Dental Sciences, Kagoshima, Japan, †Department of Experimental Therapeutics, Translational Research Center, Kyoto University Hospital, Kyoto, Japan, ‡Division of Gastroenterology and Hematology, Department of Internal Medicine, Faculty of Medicine, University of Miyazaki, Miyazaki, Japan, §Division of Gastroenterology, Imamura Hospital, Kagoshima, Japan.

Supported in part by grants-in-aid to the Research Committee of Inflammatory Bowel Disease from the Ministry of Health, Labour and Welfare of Japan.

Reprints: Hirofumi Uto, 8-35-1 Sakuragaoka, Kagoshima, Kagoshima, 890-8520, Japan (e-mail: hirouto@m2.kufm.kagoshima-u.ac.jp).

DOI 10.1002/ibd.20854

Published online 23 December 2008 in Wiley InterScience (www.interscience.wiley.com).

Host defense processes, which rely on both innate and adaptive immune mechanisms, are critical for the development of IBD.[1,2] Innate immunity participates in the activation of antigen-specific adaptive immune responses, including the production of antimicrobial peptides/proteins. In mammals, defensins, a class of antimicrobial peptides, can be divided into 2 major groups: α-defensins and β-defensins.[9] Six types of α-defensins have been identified, 4 of which are produced predominantly by neutrophils and phagocytes and stored in the granules of these cell types (denoted human neutrophil peptides 1–4; HNP 1–4). The remaining 2 α-defensins are localized in Paneth cell granules (denoted human α-defensins 5 and 6; HD 5 and 6). Although the amino-acid sequences of HNP 1, HNP 2, and HNP 3 are very similar, the sequence of HNP 4 is different than those of HNP 1–3. HD 5 is expressed by metaplastic Paneth cells in the colons of patients with UC or CD. The expression levels of HD 5 in blood, however, have not been examined; there are currently no data evaluating HNP 1–3 expression in patients with IBD.

In this study we clearly demonstrate serum profiling with increased levels of HNP 1–3 in the sera of patients with UC using a proteomics-based approach. We also compared the protein levels of HNP 1–3 in plasma samples from patients with UC and Crohn's disease (CD), before and after treatment for UC, and in patients in which treatment was effective or not effective. These analyses will contribute to our understanding of the pathogenesis of UC and aid in the discovery novel biomarkers to assess disease activity and therapeutic responses.

MATERIALS AND METHODS

Patients

After obtaining written informed consent, we analyzed a total of 94 blood samples from patients with IBD, colorectal cancer (CRC), infectious colitis, and control subjects. Forty-eight patients were diagnosed with UC (20 females and 28 males; median age, 39 years; age range, 12–72 years) and 22 with CD (11 females and 11 males; 29 years; 16–57 years). The control group contained 13 healthy subjects (5 females and 8 males; median age 30 years; age range, 24–34 years) and 5 with CRC (1 female and 4 males; median age 62 years; age range, 52–80 years) and 6 with infectious colitis (3 females and 3 males; median age 42 years; age range, 17–77 years). The study protocol was approved by the Ethics Committee of the Kagoshima University Graduate School of Medical and Dental Sciences (Kagoshima, Japan) and the Faculty of Medicine at the University of Miyazaki (Miyazaki, Japan). All IBD patients were diagnosed using established endoscopic, radiological, histological, and clinical criteria. The inactive or remission phase of UC was defined as a UCDAI score less than or equal to 2, whereas the active phase was defined as a UCDAI score greater than or equal to 3.[5] Twenty and 28 patients with UC were identified as inactive-phase and active-phase patients, respectively. All of the patients with active-phase UC were treated with oral corticosteroids, whereas 23 received leukocytapheresis therapy (LCAP) (Table 1). Furthermore, 4 of the active UC patients did not respond to treatment and eventually underwent a total colectomy. Fourteen patients with CD had high disease activities based on an International Organization for the Study of Inflammatory Bowel Disease (IOIBD) score of 2 or greater[10] and were regarded as active-phase patients. Eight patients that had lower IOIBD scores (0 or 1) were defined as inactive-phase patients. All 5 CRC patients were diagnosed with Duke's A group cancers by endoscopic, radiological, and histological examinations. All 6 patients with infectious colitis had diarrhea and fever, and were diagnosed based on clinical findings.

SELDI-TOF/MS

We used chips with cationic surfaces for analysis (CM10; Bio-Rad Laboratories, Hercules, CA). Serum samples were denatured in urea buffer (7 M urea, 2 M thiourea, 4% CHAPS, 1% dithiothreitol, and 2% ampholites), and then diluted 1:9 in binding/washing buffer (50 mM sodium acetate, pH 4). After washing the chip twice in binding/washing buffer, we applied 100 μL of diluted serum to each chip spot. Samples were incubated for 40 minutes and washed 3 times. After rinsing the chips once in water, 0.5 μL CHCA (α-cyano-4-hydoroxycinnamic acid; Nacalai Tesque, Kyoto, Japan) was applied twice to each spot and allowed to air-dry. Arrays were analyzed using a ProteinChip Reader (ProteinChip Biology System II; Bio-Rad Laboratories). TOF spectra were generated with laser shots collected in positive mode. The laser intensity ranged from 190 to 195 with a detector sensitivity of 6. On average, 65 laser shots per spectrum were used. A mixture of standard mass calibrant proteins (All-in-one Peptide Standard; Bio-Rad Laboratories) in 500 nL was used to calibrate the system for mass accuracy. The standards were applied to a single spot of the normal phase chip array (NP20; Bio-Rad Laboratories), after which two 1.0-μL samples of saturated CHCA were applied. TOF values were compared to the molecular masses of the standard proteins; calibration was performed according to the manufacturer's instructions.[7]

Immunodepletion Assay

Initially, 6 μL of anti-HNP 1–3 antibody solution (120 ng; Hycult Biotechnology, Netherlands) was bound to 30 μL of Protein A–agarose (Sigma Chemical, St. Louis, MO) for 15 minutes on ice. The postcentrifugation supernatant was discarded and the pellet was washed twice in buffer containing 20 mM HEPES (pH 7.8), 25 mM KCl, 5 mM $MgCl_2$, 0.1 mM EDTA, and 0.05% NP40. Then 15 μL of sera from each patient with UC was incubated with a pellet for 45 minutes on ice. As a negative control, samples were incubated with

TABLE 1. Characteristics of Patients with UC or CD

	UC		CD	
Disease activity[a]	Active	Inactive	Active	Inactive
Number	28	20	14	8
Gender (M/F)	19/9	9/11	10/4	6/2
Age (range), yr	41 ± 16 (14–68)	31 ± 16 (12–72)	32 ± 13 (16–57)	28 ± 7 (18–40)
Disease duration (range), yr	5.6 ± 4.8 (1–19)	5.2 ± 4.3 (1–18)	9.4 ± 7.4 (3–22)	6.0 ± 3.8 (1–13)
Treatment[b]				
5-aminosalicylic acid	28	19	14	8
Corticosteroid	28	7	10	2
Leukocytapheresis	23	0	0	0
Type of UC				
Left-side colitis	4	8	—	—
Pancolitis	24	12	—	—
Type of CD				
Ileal	—	—	4	2
Ileocolonic	—	—	9	5
Colonic	—	—	1	1

UC, ulcerative colitis; CD, Crohn's disease. Data are shown as the means ± SD or range.
[a]Active UC is defined as an Ulcerative Colitis Disease Activity Index score equal to or greater than 3, and active CD is defined as an International Organization for the Study of Inflammatory Bowel Disease score equal to or greater than 2.
[b]Includes the overlap treatment.

Protein A–agarose in the absence of a specific antibody. After incubation, samples were cleared by centrifugation; 3 μL of each supernatant was analyzed on NP20 ProteinChip arrays using a PBS II reader.[11]

ELISA

We determined the HNP 1–3 (P59665, P59666) concentrations in plasma using a human HNP 1–3 ELISA kit (Hycult Biotechnology) according to the manufacturer's instructions. Samples were analyzed in duplicate using a plate reader (Bio-Rad Laboratories) at 450 nm. The concentration of each protein in the plasma was calculated according to a standard curve.

Immunohistochemical Studies

HNP 1–3 expression in colon tissue was evaluated using immunohistochemistry. Abnormal colon tissues were obtained by total colectomy in patients with UC, whereas normal colon tissues were isolated in surgical resections for colon cancer by taking surrounding normal tissue without malignant cells. Colon tissues were fixed in 10% formalin and embedded in paraffin. For histological examination, 5-μm slices were stained with hematoxylin and eosin (HE). The anti-HNP 1–3 monoclonal antibodies (BMA Biochemicals, Augst, Switzerland) was diluted to a final concentration of 0.5% (w/v) in phosphate-buffered saline (PBS) supplemented with 1% fetal bovine serum (FBS). Immunohistochemical analysis of paraffin-embedded sections using antibodies against HNP 1–3 was performed as described.[12] EnVision plus horseradish peroxidase (Dako, Carpinteria, CA) was applied to samples; chromatin 3',3'-diaminobenzidine was used to detect bound antibody.

Statistical Analysis

Values shown are the means ± SD. Statistical significance, including that for differences in laboratory data and individual peaks in SELDI-TOF/MS, was determined using Mann–Whitney *U*- and paired *t*-tests. *P*-values < 0.05 were considered to be statistically significant. The discriminatory power for each putative marker was described via the area under the curve (AUC) from receiver operating characteristic (ROC) analysis. The statistical analyses were performed using StatView 4.5 software (Abacus Concepts, Berkeley, CA), SPSS software (SPSS, Chicago, IL), and Ciphergen ProteinChip Software (Fremont, CA) v. 3.0.2.

RESULTS

Profiling Serum Proteins in Patients with UC

We performed differential profiling of serum proteins in 11 patients with UC and 7 normal healthy controls using the SELDI ProteinChip system. Peaks were automatically detected using Ciphergen ProteinChip Software 3.0.2.[7,13] Twenty-seven serum peaks in the 3000–10,000 m/z range

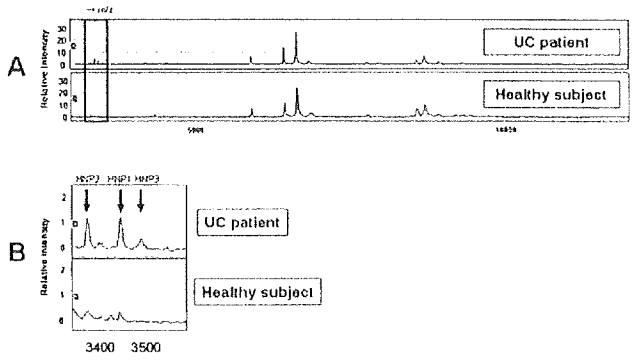

FIGURE 1. Serum proteomics of UC patients and healthy controls using SELDI-TOF/MS. (A) Spectra representing the serum proteins of a patient with UC and a healthy volunteer. The horizontal axis shows a range from 3000 to 10,000 m/z. Significant differences in peak intensities between patients with UC and healthy volunteers were found for 27 peaks. (B) The intensities of the protein peaks are shown for the range between 3300 and 3600 m/z. Protein peaks with m/z values of 3371, 3443, and 3486 represent HNP 2, HNP 1, and HNP 3, respectively.

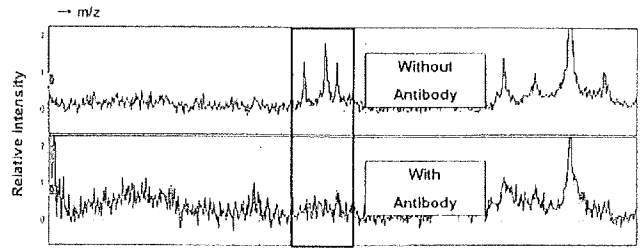

FIGURE 2. Immunodepletion assay using Protein A beads. Anti-HNP 1–3 antibodies (Hycult Biotechnology) were bound to 30 μL of Protein A beads. Sera from UC patients were incubated with these beads. After clearing by centrifugation, 3 μL of each supernatant was analyzed using an NP20 ProteinChip array.

were significantly different between the 2 patient groups (Fig. 1). Sixteen peaks resulted in *P*-values less than 0.01 (Table 2). The most dramatic difference was detected for a 3371 m/z protein, the level of which was increased in the sera of UC patients compared with healthy controls.

Identification of HNP 1–3

A previous study of colon tumor tissue identified a similarly increased signal at 3371 m/z using ProteinChip arrays.[12,14] The peak was confirmed to correspond to HNP 2 with an immunodepletion assay. Peaks at 3443 and 3486 m/z, reported to correspond to HNP 1 and HNP 3 in the previous report, were also found to be significantly increased in analyses of the sera of UC patients compared to results observed for control samples. HNP 1, 2, and 3 have similar structures consisting of 30, 29, and 30 amino acids, respectively; 29 of the amino acids are identical among the peptides.[12,15] We also subjected the serum samples to immunodepletion assays using monoclonal antibodies against HNP 1–3 and found that the 3371, 3443, and 3486 m/z protein peaks in the SELDI-TOF MS spectra were no longer observed for the sera from patients with UC (Fig. 2). These peaks were clearly observed for negative control samples, which underwent immunodepletion assays in the absence of specific antibodies. These results indicate that the 3371, 3443, and 3486 m/z

TABLE 2. Discriminatory Peaks and Mean Values in Samples from Patients with Ulcerative Colitis and Healthy Volunteers

Mass to Charge (m/z)	Ulcerative Colitis (n = 11)	Healthy Subject (n = 7)	P-value
3371	1.42 ± 0.66	0.40 ± 0.10	4.8×10^{-4}
4789	0.51 ± 0.82	0.05 ± 0.03	4.8×10^{-4}
5421	0.34 ± 0.24	0.09 ± 0.02	4.8×10^{-4}
8688	0.65 ± 0.41	1.70 ± 0.38	6.8×10^{-4}
5838	0.79 ± 0.85	0.21 ± 0.05	9.4×10^{-4}
4351	0.82 ± 0.62	2.21 ± 0.56	1.3×10^{-3}
5620	0.11 ± 0.05	0.39 ± 0.23	1.7×10^{-3}
6881	1.00 ± 0.59	2.24 ± 0.46	1.7×10^{-3}
9358	0.17 ± 0.06	0.80 ± 0.52	1.7×10^{-3}
7023	0.12 ± 0.07	0.66 ± 0.46	2.4×10^{-3}
4469	3.31 ± 2.16	1.02 ± 0.59	3.2×10^{-3}
4542	0.39 ± 0.17	0.16 ± 0.02	4.3×10^{-3}
4590	0.86 ± 0.45	1.63 ± 0.26	4.3×10^{-3}
4287	0.68 ± 0.37	1.26 ± 0.39	5.7×10^{-3}
2900	0.18 ± 0.12	0.37 ± 0.14	9.8×10^{-3}
2979	1.00 ± 0.88	0.26 ± 0.15	9.8×10^{-3}

Statistical significance was determined using a Mann-Whitney *U*-test.

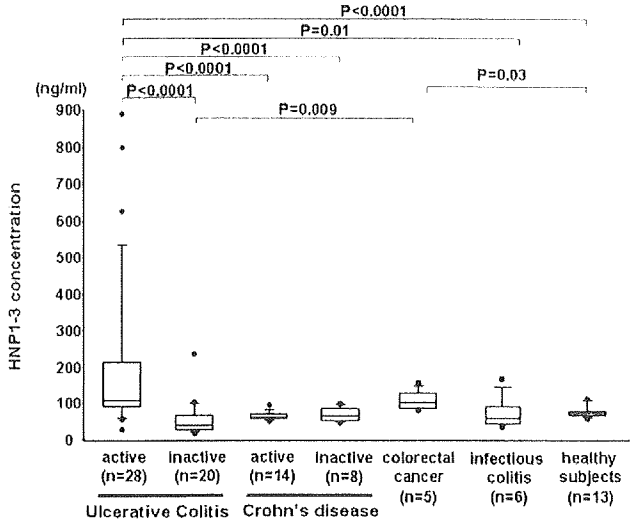

FIGURE 3. Concentrations of HNP 1–3 in the plasma of patients with UC, CD, colorectal cancer, infectious colitis, and healthy controls. Boxes indicate the median ± 25th percentile. The lower bar indicates the 10th percentile and the upper bar indicates the 90th percentile.

protein peaks, which were larger in the spectra for sera of UC patients, corresponded to HNP 1–3.

Concentrations of HNP 1–3 in Plasma

It was not possible to determine the individual concentrations of HNP 1, 2, or 3 using commercially available ELISA kits; therefore, we evaluated the total concentration of HNP 1, 2, and 3 in plasma. We found that there was a clear correlation between the serum HNP 1–3 peak intensities determined using the SELDI system and the plasma HNP 1–3 concentration measured using ELISAs in 11 patients with UC and 7 normal controls (r = 0.68, P < 0.01). We then determined the plasma concentrations of HNP 1–3 in 48 UC patients, 22 CD patients (Table 1), 5 CRC patients, 6 infectious colitis patients, and 13 healthy controls (Fig. 3). The plasma concentrations of HNP 1–3 were significantly higher in patients with active UC (203.1 ± 215.5 ng/mL) than in patients with inactive UC (58.3 ± 49.5 ng/mL), CD (active; 65.5 ± 11.2 ng/mL, inactive; 70.4 ± 20.0 ng/mL), infectious colitis (72.2 ± 16.5 ng/mL), or the healthy controls (77.5 ± 16.4 ng/mL). In addition, HNP 1–3 concentrations in patients with active UC tended to be higher in patients with CRC at Duke's stage A (100.8 ± 27.6 ng/mL), but not significantly. HNP 1–3 concentrations in CRC patients were also higher than those in patients with inactive UC and healthy controls.

Expression of HNP 1–3 in Intestinal Tissue

We examined the localization of HNP 1–3 in normal tissues and those from patients with active-phase CD or UC using immunohistochemistry. The colonic mucosa, lamina propria, muscle layer, and crypt abscesses of patients with active UC exhibited strong staining with anti-HNP 1–3 antibodies (Fig. 4). These sections contained a number of infiltrating neutrophils (Fig. 4B,C), which may provide a source of the secreted HNP 1–3 near the colonic epithelium. Positive staining for neutrophils, however, was seen in the blood vessels of both normal and abnormal colon tissues. In addition, small numbers of neutrophils with positive staining were seen in submucosal tissue of patients with CD (Fig. 4D). Epithelial cells in colon samples from patients with inflamed CD or from normal healthy subjects did not exhibit staining with anti-HNP 1–3 antibodies (Fig. 4D,E).

HNP 1–3 as a Biomarker in UC Patients

We investigated the association between the HNP 1–3 concentration and the clinical course of UC. We determined the HNP 1–3 concentrations in pairs of plasma samples from 15 patients with active UC obtained before and after induction therapy with corticosteroids (Table 3). Eight UC patients in the responder group were successfully treated by induction therapy. The elevated HNP 1–3 levels of UC patients in the responder group were reduced after induction therapy (Fig. 5). In contrast, 7 patients in the nonresponder group, 2 of whom had a total colectomy and 5 who quickly relapsed, were not effectively treated. The HNP 1–3 levels of patients in the nonresponder group before treatment were lower than those in the responder group and were not changed after treatment (Fig. 5). Additionally, although plasma HNP 1–3 levels (means ± SD) of responder active UC patients (273.0 ± 224.8 ng/mL) were higher than those with active CD (65.5 ± 11.2 ng/mL) (P < 0.001), those with nonresponder active UC (84.6 ± 26.5 ng/mL) were similar to those with active CD. These results indicate that patients with active UC and low HNP 1–3 levels do not respond well to treatment.

We evaluated the relationship between the HNP 1–3 levels and the clinical activity of UC. There was a significant correlation between the HNP 1–3 levels and the UCDAI score or the white blood cell count (WBC) of UC patients (r = 0.54, P < 0.01; r = 0.55, P < 0.01, respectively), although no correlation between the HNP 1–3 levels and the C-reactive protein (CRP) levels was noted (r = 0.24). In addition, ROC analysis was performed to estimate the efficiency of induction therapy for patients with active-phase UC; we calculated the sensitivity and specificity of HNP 1–3 levels for discriminating responder UC patients from nonresponders. We obtained a sensitivity of 89% and a specificity of 80% using a cutoff value of 100 ng/mL HNP 1–3; the ROC AUC was 0.89 between the responder and nonresponder groups of UC patients. For evaluations of the activity of UC, we compared such inflammatory markers as the CRP level and the WBC to the HNP 1–3 level in patients with UC. ROC AUC of the CRP level and WBC were 0.76 and 0.56, respectively. Thus,